

AD-A122 432

MEASUREMENTS OF THE FLOW FROM A HIGH SPEED COMPRESSOR  
ROTOR USING A DUAL..(U) NAVAL POSTGRADUATE SCHOOL  
MONTEREY CA R SHREEVE ET AL. SEP 82 NPS67-82-010

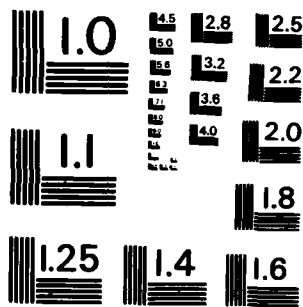
1/1

UNCLASSIFIED

F/P 20/4

NL

END  
DATE  
FILMED  
183  
DTIC



MICROCOPY RESOLUTION TEST CHART  
NATIONAL BUREAU OF STANDARDS-1963-A

②

NPS67-82-010

# NAVAL POSTGRADUATE SCHOOL

## Monterey, California



AD A 122 432

FILE COPY

MEASUREMENTS OF THE FLOW FROM A HIGH SPEED  
COMPRESSOR ROTOR USING A DUAL PROBE  
DIGITAL SAMPLING (DPDS) TECHNIQUE

R. Shreeve  
F. Neuhoﬀ

September 1982

Interim Report; October 1980 - September 1982

Approved for public release; distribution unlimited

Prepared for:  
Office of Naval Research  
800 North Quincy Street  
Arlington, Virginia 22217

DTIC  
SELECTED  
DEC 16 1982  
F

82 12 16 035

NAVAL POSTGRADUATE SCHOOL  
Monterey, California

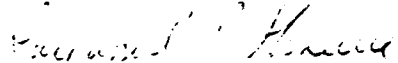
Rear Admiral J. J. Ekelund  
Superintendent


David A. Schrady  
Provost

The work reported herein was supported by Project Squid and the Power Program, Office of Naval Research under the cognizance of J. R. Patton Jr. and Dr. A. D. Wood. Support for the facility was through the Transonic Compressor Program sponsored by Naval Air Systems Command under the cognizance of Dr. G. Heiche.

Reproduction of all or part of this report is authorized.


This report was prepared by:


  
R. SHREEVE  
Director  
Turbopropulsion Laboratory

  
F. NEUHOFF  
Project Engineer  
BDM Corporation

Reviewed by:

Released by:

  
D. M. LAYTON  
Acting Chairman  
Department of Aeronautics

  
WILLIAM M. TOLLES  
Dean of Research

## UNCLASSIFIED

SECURITY CLASSIFICATION OF THIS PAGE (When Data Entered)

REPORT DOCUMENTATION PAGE		READ INSTRUCTIONS BEFORE COMPLETING FORM
1. REPORT NUMBER NPS67-82-010	2. REPORT ACCESSION NUMBER A122 432	3. RECIPIENT'S CATALOG NUMBER
4. TITLE (and Subtitle) Measurements of the Flow from a High Speed Compressor Rotor Using a Dual Probe Digital Sampling (DPDS) Technique	5. TYPE OF REPORT & PERIOD COVERED Interim Report Oct. 1980 - Sept. 1982	
7. AUTHOR(s) R. Shreeve F. Neuhooff	6. PERFORMING ORG. REPORT NUMBER	
9. PERFORMING ORGANIZATION NAME AND ADDRESS Naval Postgraduate School Monterey, California 93940	8. CONTRACT OR GRANT NUMBER(s)	
11. CONTROLLING OFFICE NAME AND ADDRESS Office of Naval Research 800 North Quincy Street Arlington, Virginia 22217	10. PROGRAM ELEMENT, PROJECT, TASK AREA & WORK UNIT NUMBERS 61153N RR024-03-01	
14. MONITORING AGENCY NAME & ADDRESS (if different from Controlling Office) Naval Postgraduate School Monterey, California 93940	12. REPORT DATE September 1982	
	13. NUMBER OF PAGES	
	15. SECURITY CLASS. (of this report) Unclassified	
	15a. DECLASSIFICATION/DOWNGRADING SCHEDULE	
16. DISTRIBUTION STATEMENT (of this Report)  Approved for public release; distribution unlimited		
17. DISTRIBUTION STATEMENT (of the abstract entered in Block 20, if different from Report)		
18. SUPPLEMENTARY NOTES		
19. KEY WORDS (Continue on reverse side if necessary and identify by block number)  Compressor Measurements Rotor Flows Dual Probe Digital Sampling		
20. ABSTRACT (Continue on reverse side if necessary and identify by block number)  The flow from a high speed rotor in a rotor-first arrangement has been measured using a "dual-probe, digital sampling (DPDS)" technique. The flow field was found to be steady in rotor coordinates (periodic in machine coordinates) outside the rotor wake, and 3 components of velocity and the pressure field were determined in this area. The wake regions were unsteady. In these regions the measurements based on ensemble		

DD FORM 1 JAN 73 1473

EDITION OF 1 NOV 65 IS OBSOLETE  
S/N 0102-014-6601

1

UNCLASSIFIED

SECURITY CLASSIFICATION OF THIS PAGE (When Data Entered)

**UNCLASSIFIED**

SECURITY CLASSIFICATION OF THIS PAGE (When Data Entered)

averages of multiple samples did not follow the behavior established in steady uniform flow except near the wake center. The broadening of the wake and three dimensional effects in the flow field were measured at reduced throttle and increased speeds. The potential for the measurement technique is discussed in some detail.

**UNCLASSIFIED**

SECURITY CLASSIFICATION OF THIS PAGE (When Data Entered)

ABSTRACT

The flow from a high-speed rotor in a rotor-first arrangement has been measured using a dual-probe, digital sampling (DPDS) technique. The flow field was found to be steady in rotor coordinates (periodic in machine coordinates) outside the rotor wake, and 3 components of velocity and the pressure field were determined in this area. The wake regions were unsteady. In these regions the measurements based on ensemble averages of multiple samples did not follow the behavior established in steady uniform flow except near the wake center. The broadening of the wake and three dimensional effects in the flow field were measured at reduced throttle and increased speeds. The potential for the measurement technique is discussed in some detail.

Accession For	
NTIS GRA&I	<input checked="" type="checkbox"/>
DTIC TAB	<input type="checkbox"/>
Unannounced	<input type="checkbox"/>
Justification	
By	
Distribution/	
Availability Codes	
Dist	Avail and/or Special
A	



## TABLE OF CONTENTS

I.	INTRODUCTION . . . . .	8
II.	DPDS MEASUREMENT APPROACH . . . . .	11
	Concept . . . . .	11
	Data Reduction Methods . . . . .	13
	Method 1 . . . . .	14
	Method 2 . . . . .	14
	Method 3 . . . . .	15
III.	EXPERIMENTAL PROGRAM . . . . .	15
	Summary . . . . .	15
	Probe Calibration and Verification . . . . .	17
	Compressor Measurements . . . . .	21
	Compressor . . . . .	21
	Test Procedure . . . . .	22
	Data Reduction . . . . .	23
	Results and Discussion . . . . .	25
	First Generation Probe System . . . . .	25
	Second Generation Probe System . . . . .	28
	Verification of the Measurements . . . . .	28
	Assumptions and Sources of Error . . . . .	30
IV.	CONCLUSIONS . . . . .	32
	TABLES . . . . .	34
	FIGURES . . . . .	36
	LIST OF REFERENCES . . . . .	57
	INITIAL DISTRIBUTION LIST . . . . .	59



## LIST OF TABLES

- I. Errors in Surface Approximation of Probe Calibration  
Data . . . . . 34
- II. Errors Obtained in Verification Tests in Steady Flow 35

## LIST OF FIGURES

1.	Arrangement of Probes in the Compressor . . . . .	36
2.	Probe Geometries . . . . .	36
3.	Synchronized Sampling Technique . . . . .	36
4.	Data Acquisition System . . . . .	37
5.	Examples of Data from the Type A Probe . . . . .	38
6.	Total Ensemble Averaged DPDS Data Acquired at One Radial Position for Two Blade Passages . . . . .	39
7.	Example of Data at One Blade-to-Blade Location . .	40
8.	Second Generation Probe Tip Geometry . . . . .	41
9(a).	Type A Probe Calibration Data at $M = 0.4$ and 9 Pitch Angles from $-15^\circ$ to $+25^\circ$ . . . . .	42
9(b).	Type B Probe Calibration Data at $M = 0.4$ and 9 Pitch Angles from $-15^\circ$ to $+25^\circ$ . . . . .	43
10(a).	Calibration Surface for Dimensionless Velocity . .	44
10(b).	Calibration Surface for Pitch Angle . . . . .	45
11.	Views of the Combination Probe (Left--with Thermo- couple Sensor Removed. Right--Thermocouple Sensor) . . . . .	46
12.	Probe Orientation and Blade Geometry at the Outer Case Wall . . . . .	47
13.	Compressor Stage Performance at 50, 60 and 70% of Design Speed (30,460 RPM) . . . . .	48
14(a).	Flow Field from Compressor Rotor Using DPDS Tech- nique at 50% Speed Near Peak Efficiency--Results for Dimensionless Velocity . . . . .	49
14(b).	Flow Field from Compressor Rotor Using DPDS Tech- nique at 50% Speed Near Peak Efficiency--Results for Yaw Angle . . . . .	50

14(c).	Flow Field from Compressor Rotor Using DPDS Technique at 50% Speed Near Peak Efficiency--Results for Pitch Angle . . . . .	51
15.	Measurements at Mid Span at 50% Speed (RUN 116, near peak efficiency) . . . . .	52
16.	Velocity Diagrams for Different Blade-Blade Positions . . . . .	53
17.	Relative Flow Velocity Distribution at Mid Span Deduced from Absolute Measurements (RUN 116) . . .	54
18.	Second Generation Probe Measurements at Mid Span at 60% Speed (— RUN 123, peak eff; ... RUN 125, throttled) . . . . .	55
19.	Pressure Coefficient vs Yaw Angle for Type A Probe at Specific Blade-to-Blade Positions (Run 123. Solid Line is from Calibration at $m = 0.4$ , $\phi = 0^\circ$ )	56

## I. INTRODUCTION

Axial compressor design systems, involving iterations between axi-symmetric and blade-to-blade calculations and incorporating empirical representations for losses, have been remarkably successful in producing high performance machines, even when the internal flow conditions are transonic. Examples exist today of commercially successful compressors with multiple transonic stages. However, the situation remains that the full range of performance of an entirely new compressor of advanced design can not be predicted reliably before the machine is tested, nor can the steady and unsteady loads on the blades be predicted with sufficient accuracy to guarantee flutter-free operation and to allow the use of minimum structural weight. As a consequence, compressor development follows an evolutionary procedure in which problems are discovered and remedied through testing.

Clearly, analysis programs are needed which adequately describe the detailed behavior of the flow in high speed compressor stages. The difficulties however are enormous; the flow field involves embedded shock waves in the presence of boundary layers, leakage flows and adverse pressure gradients and passes from rotating to stationary blade rows. Since several of the elemental processes are still lacking a fundamental description, and since the three dimensional and

unsteady nature of the flow is inherent, it is quite unlikely that an analysis which is totally devoid of "modelling" approaches will be possible in the foreseeable future. Consequently, in order to develop computational codes for compressor analysis which are both realistic and useful, it is of paramount importance to determine experimentally and concurrently the actual flow field in stage geometries to which the developing analyses can be applied. While such an activity has sometimes been labelled "code verification", it is more likely in fact that some experimental information will be needed during the process of code development. For example, the mechanism responsible for the unreasonably high losses observed in the outer 30% of several transonic rotors <sup>(1)</sup> is unlikely to be resolved by purely analytical approaches.

The present work follows the above arguments. It reports the first results in a program aimed at the determination of the flow field produced by a single compressor rotor in a rotor-first arrangement. Computation of the rotor flow using recently developed codes <sup>(2)</sup> is intended, however only the experimental program is reported herein.

A small, 450 HP transonic single-stage axial compressor and test rig designed for continuous operation has been used. The rig was built to facilitate detailed measurements of internal flow behavior and specifically to provide the means to obtain information with which to verify and help improve methods of flow computation. The present stage is one of

in-house design.<sup>(3)</sup> Instrumentation was developed and applied first to measure time-averaged flow behavior through the compressor.<sup>(4)</sup> Then concentration was placed on the determination of the detailed internal aerodynamics. Clearly, in order to measure the unsteady flow field one must either use high response probes or an optical technique of some kind. While non-intrusive laser velocimetry techniques had many advantages, it was clear that they required an expert to apply them in each new situation, and they were normally able to measure only two components of the velocity. They did not provide measurements of the pressure field, and in highly unsteady flows the accuracy was questioned. There was good reason therefore to approach the problem of measuring the unsteady flow field in other ways, and ideally to obtain independent, redundant measurements of the same phenomena. The work reported here was such an attempt.

Synchronized (phase-locked) digital sampling from Kulite transducers was adopted as a technique for defining both case wall pressure signatures and the exit flow field from the rotor. Early results were reported and a method was proposed in Ref. 5 for obtaining the full periodic velocity field at the rotor exit from measurements with two very simple Kulite probes. The present paper reports the first distributions measured of the velocity vector (magnitude, yaw angle and pitch angle) across two rotor blade passages in both hub-to-shroud and blade-to-blade directions, made using the proposed

technique. The report describes the measurement approach and gives an account of the experimental procedures used. Results are presented and are discussed first on the basis of their qualitative behaviour, and then for their quantitative accuracy.

Since measurement redundancy was inherent in the approach, it could be shown definitively that the measurements obtained in regions of the flow which were periodic in the machine frame (steady with respect to the rotor) were reliable, whereas measurements obtained in the unsteady (wake) regions could not be interpreted accurately on the basis of probe calibrations obtained in a steady flow. The full implications of these observations are discussed in detail.

## II. DPDS MEASUREMENT APPROACH

### Concept

Two Kulite semi-conductor pressure probes of very simple design are positioned behind the compressor rotor as shown in Fig. 1. The "Type A" and "Type B" probes, shown in Fig. 2, are mounted eccentrically in plugs so that they can be rotated about the centers of their tips. Data from each probe is digitized under "Pacer" control. Inputs to the Pacer are one-per-blade and one-per-rev. signals obtained as shown in Fig. 3. The complete data system, based on a Hewlett-Packard HP21MX computer, is shown in Fig. 4. The Pacer allows the data to be converted at any point in the rotor's rotation by internally generating a pulse train with a frequency which is phase-locked

to the blade passing frequency but multiplied by a factor of 128. Conversion is controlled to occur when a programmed number of counts matches the number of pulses counted by the Pacer from the one-per-rev. reset pulse.

The Pacer control allows data to be digitized from each probe when it is at precisely the same location with respect to the rotor blading. In effect, two differently oriented sensors (Type A and Type B) can be sampled at the same point in the rotor frame of reference. However, since each probe can also be rotated about its tip, data can also be obtained (at each rotor point, blade-to-blade) as a function of the sensor yaw angle. In practice, data are taken at each of 256 points across adjacent pairs of rotor blade passages with both probes rotated in unison to from 5 to 9 separate yaw angle settings. Multiple samples (from 10 to 40) on successive revolutions are taken at each point and probe angle setting and ensemble-averaged before recording. An example of the ensemble-averaged data taken on the compressor annulus center-line across two particular blade passages with a Type A probe is shown in Fig. 5. A composite picture of the complete data obtained from the Type A and Type B probes for one radial location across two rotor blade passages is shown in Fig. 6.

The goal then is to reduce the information obtained in Fig. 6 to obtain the distribution of the velocity vector in the blade-to-blade direction.



### Data Reduction Methods

The reduction to velocity requires the following assumptions:

- i) that the probes respond with negligible error to fluctuations in the flow which are at blade-passing frequency;
- ii) that the flow is, on the average, steady in the rotor frame.

The first assumption is required since the calibration of the probes can only be carried out in a steady flow field. The second assumption is required since the two sensors are in different peripheral locations. (The validity of the assumptions will be discussed after an examination of the results.)

In general, at each point in the blade-to-blade direction there are five unknown quantities; namely, flow yaw angle, flow pitch angle, flow velocity, pressure and temperature. In all approaches followed to date, the probe's pressure response has been expressed as a function of the Mach number and it is assumed the effect of Reynolds number between the probe calibration and application is small. The unknowns at each point are then yaw angle, pitch angle, Mach number and pressure. In reducing Mach number to velocity, the stagnation temperature is assumed to be constant across the blade passage at the time averaged value measured at the rotor exit. Thus, in principle, only four independent pressure measurements are required in order to derive the properties of the flow at each point. Using 5 to 9 probe angle settings with two probes, 10 to 18 independent measurements result, so that considerable redundancy is

always present. (It should be noted that the experimental procedure described below, includes on-line calibration of the transducers to remove the effect of their temperature sensitivity.)

Three fundamentally different approaches to the data reduction have been examined. The methods are best understood with reference to Fig. 7 which shows an example of data obtained at a single point in the blade-to-blade direction (for example, any two corresponding curves in the two data sets in Fig. 6). It is assumed for the moment that the data are known as pressures after the transducer's have been calibrated, on-line.

Method 1. As reported in Ref. 6, in this method the calibration curves for the two probes are approximated by fourth order polynomials and hence the flow yaw angle (indicated in Fig. 7), and values of  $p_{A \text{ max}}$  and  $p_{B \text{ max}}$  can be found from the test data by curve fitting. The Mach number, pitch angle and static pressure are then calculated using three approximate equations to which the calibration data have previously been reduced. The values of  $p_{A \text{ max}}$ ,  $p_{B \text{ max}}$ ,  $p_A$  and  $\alpha_A$  are sufficient to determine the unknowns, and hence each data point obtained with the Type A probe which is well away from the maximum point determines a result for the flow vector.

Method 2. As reported in Ref. 7, this is a numerical iteration approach in which the calibration data are stored in arrays and any three (3) values from the Type A probe and

one (1) from the Type B probe can be used to derive the four unknowns. In principle the approach can be used if the output of the probe is not symmetric about its maximum so long as only one maximum exists.

Method 3. Reported in Ref. 8, this method is similar to that originally proposed in Ref. 5 but makes use of analytical tools developed more recently.<sup>(9)</sup> It uses the values  $p_{A \text{ max}}$ ,  $p_{B \text{ max}}$  and  $p_A$  taken at a discrete value of  $\alpha_A$  (here  $63^\circ$ ), as if they were pressures from a conventional multiple-sensor flow probe. (The values must be obtained from the data by interpolation.) It is shown in Ref. 10 that the calibration of multiple sensor probes can be well represented as two surfaces, one for Mach number, one for pitch angle as a function of two pressure coefficients defined in terms of the four individual sensor measurements. In the present application, the flow yaw angle is first derived by a curve fit to the Type B probe data and the value of  $p_A$  is taken where the right and left hand sides of the Type A characteristic are separated by 126 degrees.

The results presented in the present paper were reduced using Method 3 only.

### III. EXPERIMENTAL PROGRAM

#### Summary

The measurements reported here were made with two generations of probes. First, probes having the tip geometry shown in Fig. 2 were calibrated in a free-jet and applied in

the compressor. The probe tips were 2.36 mm (0.093 inches) in diameter and incorporated Kulite XB-093-25 transducers. As reported in Ref. 6, the outputs of both probes as a function of yaw angle could be represented well by polynomials of fourth order. It was also found during calibration that the yaw angle at which the probe indicated ambient (static) pressure was independent of Mach number. This observation led to an analytical reduction of the calibrations to simple polynomial equations. Because the symmetry of the pressure characteristic was to be used in the data reduction it was concluded at this stage that an accurately formed or machined tip geometry was required for both probes. By recasting the raw calibration data into the required form, one complete set of test data from the compressor was reduced to velocity profiles and is presented herein. Failure of the Type A probe during handling prevented further work with the first generation system. The results obtained with the first generation probes will be discussed qualitatively only since it was not possible to repeat the early calibration on which the reduction was based.

The second generation probes were smaller and the inclined angle of the Type B probe tip to the axial direction was reduced from  $55^\circ$  to  $35^\circ$ . The larger angle had been chosen initially so that the difference between Type A and Type B probe readings would be comparable to the dynamic pressure. The angle was reduced because at  $55^\circ$  the output of the Type B probe became insensitive to pitch angle at only a few degrees

of positive pitch. Each probe tip diameter was 1.57 mm (0.062 inches) and used a Kulite "Type B" screen with eight holes as shown in Fig. 8. The change in tip geometry (the larger probes had a slightly recessed screen) gave a change in the shape of the output-angle characteristic. It was also found that partial blockage of the holes in the screen (Fig. 3) caused "skewing" of the output-angle characteristic, and this was remedied before a full calibration was made.

The second generation probes were calibrated in a free jet and calibration surfaces required for the data reduction using Method 3 were generated. The calibration representation was then verified by separate free jet tests and the probes were installed on the compressor. The procedures used with the second generation probes will be described here, and the results obtained in the compressor will be analyzed for their probable accuracy.

#### Probe Calibration and Verification

A 10.16 cm (4 inch) diameter continuous free air jet exhausting to atmosphere was used for both calibration and verification tests. The apparatus is described in Ref. 8 and details of the procedures are given in Ref. 10. The probes were calibrated separately. The probe mount allowed complete rotation in yaw and variation in pitch from  $-45^{\circ}$  to  $+45^{\circ}$ . Each calibration involved recording the probe output digitally with reference data as the probe was continuously yawed from  $-80^{\circ}$  to  $+80^{\circ}$  and back at each of 9 discrete pitch angles ( $-15^{\circ}$

to  $+25^\circ$  in increments of  $5^\circ$ ) at each of 6 Mach numbers (0.2 to 0.7 in increments of 0.1). For each of the 54 combinations of pitch angle and Mach number, 300 values were obtained to describe the probe output (p) vs yaw angle ( $\alpha$ ) characteristic for each probe. Figure 9 shows examples of the calibration data obtained with the Type A and Type B probes. The average of the sweeps to and from was taken after this was verified to give a correct result.

In order to represent the calibration data in the form required by Method 3, the following procedure was followed for each value of Mach number and pitch angle:

- (i) the maximum value of the Type A probe output,  $P_{A \text{ max}}$ , was found using a 4th order polynomial curve fit to  $p_A$  vs  $\alpha_A$  for  $-20^\circ < \alpha < 20^\circ$
- (ii) the value of  $p_A$  at  $\alpha = -63^\circ$  (on the left branch and designated  $p_{SAL}$ ) was found by second order interpolation over eight data points
- (iii) the corresponding value  $p_{SAR}$  on the right branch at  $\alpha = +63^\circ$  was found using the same procedure
- (iv) the average of  $p_{SAL}$  and  $p_{SAR}$  was calculated;  $P_{SA}$
- (v) the maximum value of the Type B probe output,  $P_{B \text{ max}}$ , was found using a 4th order polynomial curve fit to  $p_B$  vs  $\alpha$  for  $-30^\circ < \alpha < +30^\circ$
- (vi) the 3 pressure coefficients,  $\beta$ ,  $\gamma$  and  $\delta$ , were calculated using the definitions

$$\beta = \frac{P_{A \text{ max}} - P_{SA}}{P_{A \text{ max}}} \quad (1)$$

$$\gamma = \frac{P_{A \text{ max}} - P_{B \text{ max}}}{P_{A \text{ max}} - P_{SA}} \quad (2)$$

$$\text{and} \quad \delta = \beta \cdot \gamma \quad (3)$$

- (vii) the dimensionless velocity  $X$ , defined as the ratio of velocity  $V$ , to "limiting" or stagnation velocity,  $V_t$ , was calculated from the relationship

$$X^2 = \frac{\frac{\gamma-1}{2} M^2}{1 + \frac{\gamma-1}{2} M^2} \quad (4)$$

where

$$X = \frac{V}{V_t} \quad (5)$$

and

$$V_t = \sqrt{2c_p T_t} \quad (6)$$

where  $c_p$  is the specific heat at constant pressure and  $T_t$  is stagnation temperature.

From these data, surface approximations of the calibration were obtained in the form

$$X = X(\beta, \gamma) = \sum_{i=1}^L \left\{ \sum_{j=1}^M c_{ij} \beta^{(j-1)} \right\} \cdot \gamma^{(i-1)} \quad (7)$$

$$\phi = \phi(\beta, \gamma) = \sum_{i=1}^L \left\{ \sum_{j=1}^M d_{ij} \beta^{(j-1)} \right\} \cdot \gamma^{(i-1)} \quad (8)$$

using subroutines given in Ref. 9. The orders of the approximation were selected as those giving the least error in approximating the data in the desired range. The results for the second generation probes are shown in Fig. 10. In effect, the calibration data are completely replaced by the coefficients  $c_{ij}$ ,  $d_{ij}$ . In reducing data from the compressor (or verification tests), the coefficients are entered into the reduction program and the values of  $X$  and  $\phi$  are obtained from measured values of  $\beta$  and  $\gamma$  using Eq. (7) and Eq. (8).

The accuracy of the reduction method and surface approximation was calculated for the data obtained in the calibration tests. The results are given in Table I for the range of interest. The errors are defined as

$$\epsilon_X = \frac{X_m - X_c}{X_m} \cdot 100 \quad (9)$$

and

$$\epsilon_\phi = \phi_m - \phi_c \quad (10)$$

where subscript m indicates the measured value and subscript c denotes the value given by Eq. (7) or Eq. (8) using the selected coefficients. Included in Table I is the error in the derived yaw angle given by

$$\epsilon_\alpha = \alpha_m - \alpha_c \quad (11)$$

where  $\alpha_m$  was  $0^\circ$  and  $\alpha_c$  was the yaw angle of the Type B probe corresponding to the maximum output,  $P_{B \max}$ . The yaw angle was defined for the compressor data in the same way.

To evaluate the probable error involved in applying the calibration to compressor test data, specific test conditions were established in the free jet and data were acquired from the two probes at the same time following the procedure to be used in the compressor. Data were taken with the probes set at nine different yaw angles between  $-65^\circ$  and  $+65^\circ$ . The data were reduced using procedures similar to those described for the compressor tests. The errors between the known (measured, subscript m) condition and that obtained using the measured data in Eq. (7) and Eq. (8) (calculated, subscript c), were



evaluated using the definitions in Eq. (9) and Eq. (10). The results are shown in Table II. It can be seen that in a steady uniform flow, the maximum uncertainty in the magnitude of the dimensionless velocity was 1.5%, in yaw angle 0.8 degrees, and in pitch angle 1.0 degrees.

#### Compressor Measurements

Compressor: The transonic compressor in which the measurements were made is a single stage machine with axial inlet flow to the rotor. Figure 1 shows the flow path to scale. The outside case wall diameter is 27.94 cm (11 inches) and the blade height is approximately 6.99 cm (2.75 inches), 4.83 cm (1.9 inches) and 4.57 cm (1.8 inches) at stations upstream of the rotor, downstream of the rotor and downstream of the stator respectively. The compressor design is described in Ref. 3 and the test rig in Ref. 11. The compressor is driven by a cold-air turbine supplied from a continuous laboratory air supply. Instrumentation is provided to measure stage performance. Radial survey probes are used ahead of and between blade rows and the case wall can be rotated to position instrumentation peripherally. A combination temperature-pneumatic probe of the type shown in Fig. 11 is positioned downstream of the rotor and is used to obtain the time average velocity vector and temperature through the calibration procedure given in Ref. 10. Data acquisition, recording and reduction uses the system shown in Fig. 4. The software is described in Refs. 12 and 18.

Pneumatic pressures are recorded using a Scanivalve, strain gauge transducer, signal conditioning and DVM to an uncertainty of  $\pm 25 \text{ N/m}^2$  (0.1 in. of water). Kulite differential transducer signal conditioning circuits output through a scanner to the DVM and through DATEL amplifiers to separate channels of a  $\pm 1.0$  volt range HP 5610 A/D converter. On-line calibration ensures an uncertainty in Kulite pressure data to  $\pm 0.002$  of the pressure equivalent of the 1 volt range, typically  $\pm 50 \text{ N/m}^2$  (0.2 inches of water).

The geometry of the rotor and stator blading at the tip is shown to scale in Fig. 12. Also shown to scale is a radial view of the probe (either Type A or Type B) and the range of yaw angles within which it is rotated in the data acquisition process. Velocity diagrams typical of the flow within and outside the rotor wake are shown. It is noted that the rotor blade profile is flat on the pressure side and is a circular arc on the suction side. The stator blades are double circular arc.

Test Procedure: The compressor speed and throttle were adjusted to produce the desired operating condition and steady-state data were recorded. The combination probe, Type A probe and Type B probe, with tips at the same radial position, were adjusted in yaw to the time average yaw angle given by the combination probe. Data were recorded for the purpose of calibrating the Kulite probes on-line since they were known to be sensitive to temperature. This required recording the

Kulite probe outputs using an integrating voltmeter when four different levels of air pressure were applied to the reference side of the transducers. The slopes of the transducers were calculated using a least squares linear fit to the five data points. This procedure was repeated later, after the data were acquired. The data were accepted only if the two values of slope were within  $\pm 1.5\%$  and mean values were used in the reduction. Paced data at 256 positions (counts) across two blade spaces were recorded using a programmed number (10 to 40) of samples at each position. Reference data for the compressor and the time-averaging combination probe, and the time average output of the Type A and Type B probes were recorded from the integrating DVM. The Paced data and reference data recording were repeated with the Type A and Type B probes yawed in unison to four angles in each direction. Angles were chosen to range from  $-70^\circ$  to  $+80^\circ$  with respect to the time average angle to accommodate the expected flow yaw angle behavior within the rotor wakes. Further details are given in Ref. 8.

Data Reduction: The slopes of the transducers were established during the data taking procedure. The intercepts were obtained for the two probes using the time-average measurements. First, from the calibration data for the probes such as are shown in Fig. 9, polynomial (surface) expressions had been derived for

$$c_{PA_0} = c_{PA_0}(\phi) = \frac{P_{A_0} - P_s}{P_t - P_s} \quad (12)$$

(which was close to unity, 4th order in  $\phi$ , depending negligibly on Mach number) and

$$c_{pB_0} = c_{pB_0}(X, \phi) = \frac{p_{B_0} - p_s}{p_t - p_s} \quad (13)$$

Here,  $c_{pA_0}$  and  $c_{pB_0}$  are pressure coefficients at zero yaw defined for the Type A and Type B probes respectively in terms of the corresponding probe pressures  $p_{A_0}$  and  $p_{B_0}$ , stagnation pressure  $p_t$  and static pressure,  $p_s$ . Using the time-averaged values for  $\phi$ ,  $X$ ,  $p_t$  and  $p_s$  obtained from the combination probe in Eq. (12) and Eq. (13), values of  $p_{A_0}$  and  $p_{B_0}$  were calculated. It was then assumed that these values corresponded to the maxima in the time-averaged output voltages obtained as a function of probe yaw angle. Thus the two intercepts were determined, and all paced-data samples from both probes could be reduced to absolute pressures.

Data obtained at each blade-to-blade location with the probes at nine different yaw angles were reduced as a set. The same procedure was carried out for each of 256 sets. First, fourth order curves were fitted to the curves of pressure vs probe angle (Fig. 7). For the Type A probe, the value of pressure  $p_{sA}$  was found at which  $126^\circ$  separated left and right branches. The maximum value,  $p_{A \max}$ , was obtained at the mid-point between the left and right branches. From the curve for the Type B probe, the maximum pressure,  $p_{B \max}$ , was derived from the curve-fit and the flow yaw angle was obtained

at the maximum. The values of  $\beta$  and  $\gamma$  were obtained using Eq. (1) and Eq. (2), and  $X$  and  $\phi$  were calculated using the calibration coefficients in Eq. (7) and Eq. (8). Mach number was obtained from a solution of Eq. (4).

#### Results and Discussion

First Generation Probe System: Results were obtained using the first generation probe system with the compressor operating at 15,230 RPM (50% of design speed) and throttled to near peak efficiency. A partial map for the stage is shown in Fig. 13, and the machine condition for the first probe data is identified there as RUN 117. Data were obtained at eight radial positions from hub to tip across two blade passages. The resulting distributions of dimensionless velocity  $X$  (defined in Eq. 5), yaw angle,  $\alpha$  and pitch angle,  $\phi$  are shown in Fig. 14. (It is noted that the limiting velocity at room temperature is approximately 760 m/sec (2500 ft/sec).) Also shown in each distribution is the time-averaged value obtained from the combination probe.

In discussing the results, it is first noted that the data are shown plotted by the computer (pen down) without smoothing. From oscilloscope observations of probe outputs, the area of the rotor blade wake (which corresponds closely to where the yaw angle is increased) was clearly unsteady. In acquiring the data, 40 separate samples were taken at each point through the wakes and 15 were taken outside the wakes. The resulting ensemble averages are seen to result

in a smooth and coherent distribution of flow characteristics throughout. It is noted that each data point shown was reduced from two sets (2 probes) of 9 ensemble averages (at each probe angle) digitized at quite different times in the acquisition process. The coherence of the behavior from point to point at a single radial position is therefore better than might have been expected. The clearly coherent changes in behavior observed with radial displacement is striking.

The agreement of the measurements with the time-average values is to be expected since the on-line calibration procedure forces the time averaged behavior of the Kulite system to duplicate that of the combination probe. However, it is noted that this simply fixes the intercepts for the transducers and the paced data from which the data in Fig. 14 was reduced was otherwise obtained independently.

Qualitatively, the yaw angle distribution is as would be expected, with increased magnitudes resulting from lower relative velocity in blade wake regions. The absolute velocity magnitude appears to vary outside the wake nearer to the hub, with larger magnitudes from the suction side of the blades. The outermost distribution was taken 4.83 mm (0.19 inches) from the case wall and was probably influenced by case wall boundary layer and tip flow effects. This is most evident in the derived pitch angle which is seen to vary as much outside as inside the blade wakes.

The qualitative behavior of the results was examined using the first successful data obtained on the annulus centerline in an earlier test. The machine condition is indicated as RUN 116 in Fig. 13. The dimensionless velocity and yaw angle results are shown in Fig. 15 and three discrete conditions to be examined at counts 47, 88 and 95 respectively are indicated. Count 47 is outside the wake, count 88 corresponds to the maximum yaw angle (which occurs at a velocity magnitude greater than the minimum). The velocity diagrams which correspond to the data at these three positions are shown in Fig. 16. It can be seen that the relative flow velocity vectors for the three positions and for the time averaged condition are at  $51^\circ$  or  $52^\circ$  ( $50.8^\circ$  was used in design). Hence a relative velocity which is almost constant in angle but wake-like in magnitude is consistent with the reduced data. It can also be seen in Fig. 16 why the minimum in absolute velocity does not occur at the maximum yaw angle. If the relative flow angle were truly constant, then the absolute velocity vector would move along the broken line drawn parallel to this direction. The minimum velocity magnitude occurs where the absolute velocity is normal to the broken line (approximately true here at count 88), whereas the maximum yaw angle occurs where the magnitude of the relative flow velocity is a minimum. Hence the behavior of the derived velocity magnitude and angle is consistent with a nearly constant relative

flow angle. The calculated distribution of the relative flow vector is shown in Fig. 17 for the data from RUN 116.

Second Generation Probe System: Data were obtained using the second generation probe system on the centerline of the compressor annulus, at 18300 RPM (60% of design speed) at different compressor flow rates. The machine run conditions were those indicated in Fig. 13. RUN 123 was taken near peak efficiency while RUN 125 was at more throttled conditions. Ensemble averages were taken over 40 samples at all blade-to-blade positions. The results are shown in Fig. 18.

It can be seen that as the compressor was throttled the average yaw angle increased, the change in yaw angle through the wake increased, and the wake width increased. There was also a significant change in pitch angle in the wake, with up to  $12^{\circ}$  positive increase indicated at the throttled condition. The pitch angle distribution outside the wake appeared to be little changed with throttling but showed greater variations than was observed at 50% speed. The velocity magnitude showed considerable change in the wake region; however, examination also showed that the variations in yaw angle and velocity magnitude remained consistent with almost constant relative flow angle for each set of data.

Verification of the Measurements: The qualitative behavior of the data has been discussed and has left few obvious questions. The question of quantitative accuracy remains. Fortunately, inherent in the measurement technique is



measurement redundancy, which allows the accuracy to be verified. The verification at a given blade-to-blade position involves an examination of whether the data obtained there at the 9 yaw angles follow the same characteristic obtained during calibration in steady flow at the corresponding Mach number and pitch angle. Such a comparison would be quite simple if Method 1 were used, since the pressure characteristics are there represented analytically. Using Method 3, with no such analytical representation it is more difficult and has been done properly only for the Type A probe.

If the output of the Type A probe is represented as a pressure coefficient,  $c_{pA}$ , defined as

$$c_{pA} = \frac{p_A - p_s}{p_t - p_s} \quad (14)$$

it is found that  $c_{pA}$  depends very little on Mach number generally, and very little on pitch angle in the range  $-5^\circ < \phi < 20^\circ$ . Thus, when the local values of  $X$  (or Mach number) and  $\phi$  have been derived, the local values of  $p_t$  and  $p_s$  are given by Eq. (12) and Eq. (13) and values for  $c_{pA}$  can be calculated using Eq. (14) for each probe yaw angle. These values can be imposed on the curve of  $c_{pA}$  vs  $\alpha$  obtained at a similar Mach number and similar pitch angle during calibration.

This has been done for data obtained in RUN 123 and the results are shown in Fig. 19. First, it can be seen that the time-averaged data obtained as a function of yaw angle closely approximated the behavior in steady flow. Also, data acquired

outside the wake region (at count 128) was also consistent with steady-flow behavior. Inside the wake, however it is clear that the behavior of the ensemble-averaged data do not follow the characteristic established in steady flow except at the very center (at count 188). Going into the wake (at count 181), the characteristic is skewed and the peak probe output is to the right. Coming out of the wake (at count 195), the characteristic is skewed, with the peak output to the left.

It must therefore be concluded that reduced data obtained outside the unsteady wake regions can be accepted to within the uncertainty derived from the measurement uncertainty. The reduced data for the area of the wake contains an unknown uncertainty for which an explanation is required. The values at the center of the wake however, appear also to be verified.

Assumptions and Sources of Error: The verification suggests that for the measurements made outside the wake, the method gives acceptable results. Several assumptions were made nevertheless, which should be examined.

The assumption that the probes respond with negligible error to fluctuations at blade passing frequencies was supported by oscilloscope observations of raw signals. The probes were observed to respond quite differently in the wake region compared to outside the wake region. The probe output fluctuated only over a clear fraction of each blade passage and was otherwise quite steady when triggered by

the one-per-rev signal. That the flow outside the wake was, on the average, steady in the rotor frame was clearly demonstrated by the same observations.

The assumption was made for the on-line calibration that the time averaged behavior of the Kulite probe system could be equated to that given by the combination probe. This was supported in the verification check above, however the result was that the absolute levels of the parameters derived from the Kulite probe system depended on the accuracy of the combination probe. Since averaging errors can occur in pneumatic probes (although as shown in Ref. 10 they are negligible for the conditions found behind the rotor at present speeds), errors in the pressure measurements of the combination probe sensors were assumed and the effect on the Kulite measurements was evaluated. It was found that assumed errors of as much as 10% in the pneumatic pressures gave rise to negligible differences in the velocity and yaw angle results, and differences ranging from  $-4^{\circ}$  to  $+1^{\circ}$  in pitch angle results.

The source of the discrepancy in the behavior of the probes in the wake regions is not resolved. It is encouraging that the measurements near the wake center may be acceptable since the knowledge of the wake width, the minimum velocity and the conditions at the wake edge are sufficient for many engineering purposes. An attempt will be made however to resolve the remaining uncertainty in the method. Of the

possible explanations, the suggestion that there is a varying temperature effect through the wake has been rejected since the thermal lag of the transducer sensor could not allow such a rapid response. The remaining potential explanations include:

- (i) the steady flow error of probe measurement in a shear layer
- (ii) differences in unsteady response at different yaw settings
- (iii) incorrect averaging procedure in a flow in which Mach number and flow angle are unsteady and probe system response is non-linearly dependent on both.

A limited attempt has been made to investigate errors which might stem from the averaging procedure. However it is difficult to see why a lack of symmetry in the probe output could be caused this way. It is noted that the error which would normally result from probe measurement in a steady shear layer is consistent with the behavior observed quantitatively, and will be investigated further. The possibility of differences in unsteady response at different yaw angles is to be investigated in the near future by changing probe tip geometry.

#### IV. CONCLUSIONS

The Dual Probe Digital Sampling (DPDS) was applied to measure the blade-to-blade and hub-to-tip flow field from two blade passages of a compressor rotor. All three components of the velocity were derived with relative success.

The results showed a coherent and realistic behavior near peak efficiency at 50% speed. Broadening of the wake with increased yaw and pitch angles was measured at mid span and the compressor was throttled at 60% speed. Outside the wake regions, the flow was found to be steady in the rotor frame and the data were shown through inherent measurement redundancy to be valid. Inside the wake regions, the flow was found to be unsteady in the rotor frame and the reduced data contain an unknown uncertainty except near the wake center where they are thought to be valid. Attempts are to be made to resolve the remaining uncertainty and to compare the measurements with those from an LDA system.

TABLE I. Errors in Surface Approximation  
of Probe Calibration Data

Test Condition		Approximation Error		
<u>X</u>	<u><math>\phi</math> (deg)</u>	<u><math>\epsilon_X</math> (%)</u>	<u><math>\epsilon_\phi</math> (deg)</u>	<u><math>\epsilon_\alpha</math> (deg)</u>
.1347	15.00	-1.3357	.17	- .69
.1349	10.00	- .6396	.04	- .52
.1346	5.00	.2487	- .03	- .15
.1345	0.00	1.0161	- .07	- .40
.1750	15.00	- .9074	.25	- .73
.1758	10.00	.1439	.13	- .71
.1750	5.00	.1923	- .33	- .68
.1751	0.00	.0256	- .22	- .53
.2163	15.00	.3642	.96	- .13
.2161	10.00	- .0087	.91	- .64
.2160	5.00	- .8027	.97	- .80
.2162	0.00	- .9259	1.36	-1.05
.2626	15.00	- .6210	- .36	- .16
.2624	10.00	- .4118	- .56	- .08
.2622	5.00	- .6578	.98	- .19
.2622	0.00	- .8000	- .54	- .91
.2944	15.00	- .5198	- .20	-1.01
.2945	10.00	- .8086	- .64	- .38
.2945	5.00	-1.1207	- .03	- .76
.2948	0.00	.1303	- .41	-1.16

TABLE II. Errors Obtained in Verification  
Tests in Steady Flow

Test Condition			Total Measurement Error		
<u>X</u>	<u><math>\phi</math> (deg)</u>	<u><math>\alpha</math> (deg)</u>	<u><math>\epsilon_X</math> (%)</u>	<u><math>\epsilon_\phi</math> (deg)</u>	<u><math>\epsilon_\alpha</math> (deg)</u>
.1420	0	0	-0.04	-0.04	-0.31
.1459	5	0	+1.49	-0.26	+0.11
.1459	5	0	+1.52	+0.21	-0.1
.1450	10	0	+1.28	-0.18	-0.24
.1448	15	0	-0.02	+0.18	+0.30
.170	10	0	+1.22	+0.22	-0.78
.170	10	5	-1.17	+1.03	-0.45
.170	10	10	-0.31	-0.2	-0.22
.2049	7	0	+0.53	-0.66	+0.18
.211	10	0	-0.31	-0.16	-0.2
.2052	13	0	+0.26	-0.21	-0.24

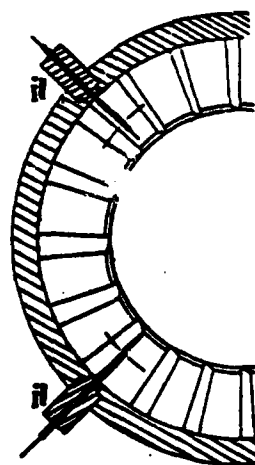
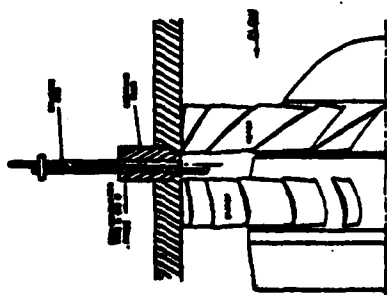
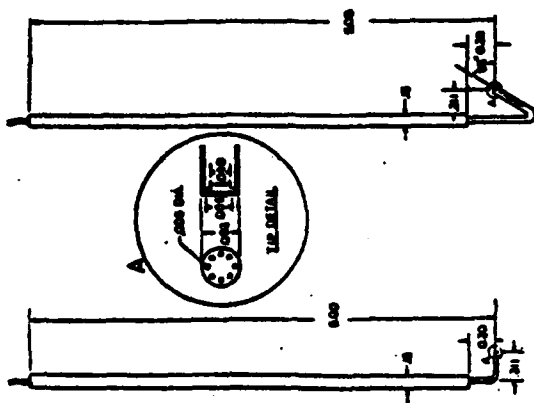


Fig. 1. Arrangement of Probes in the Compressor





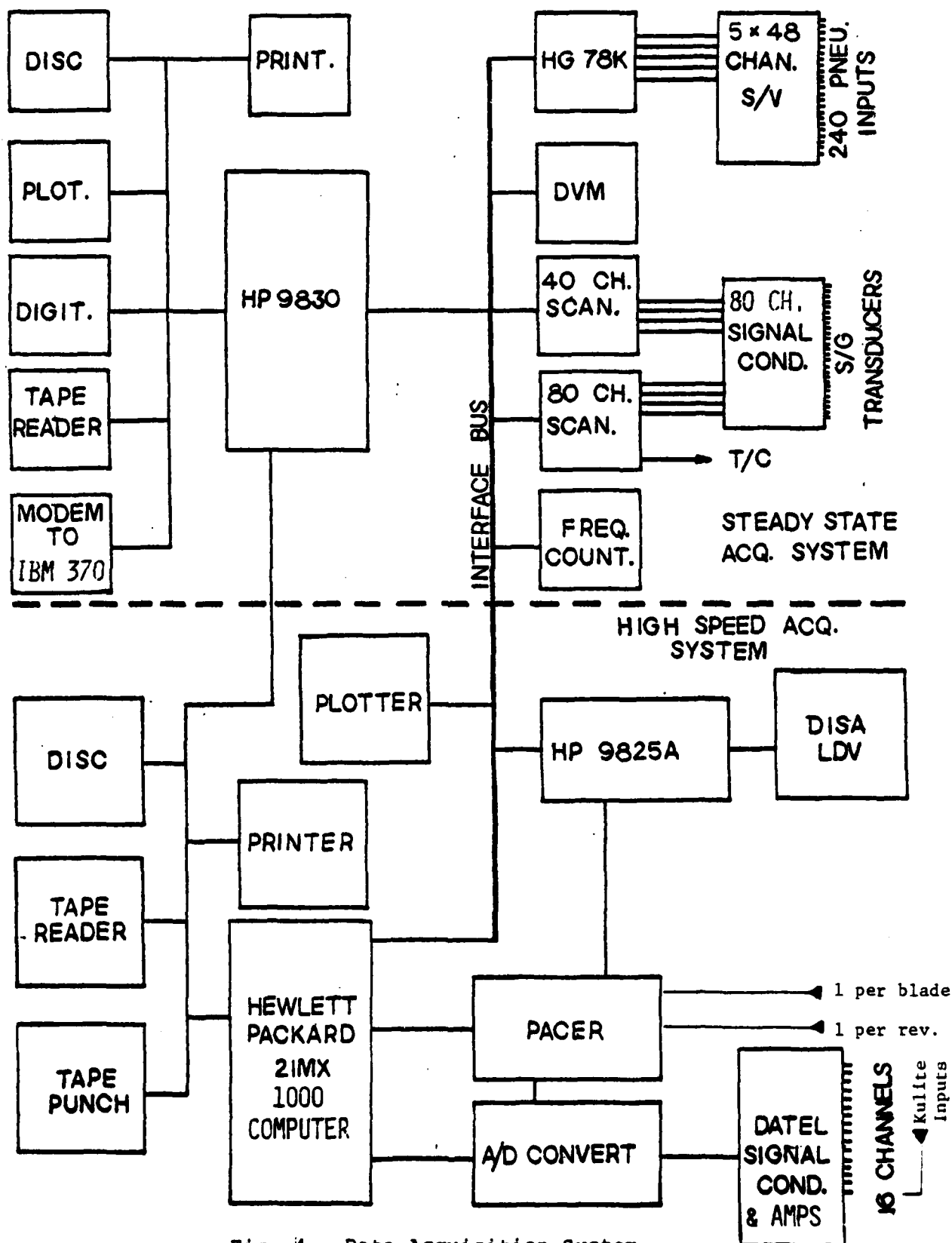


Fig. 4. Data Acquisition System

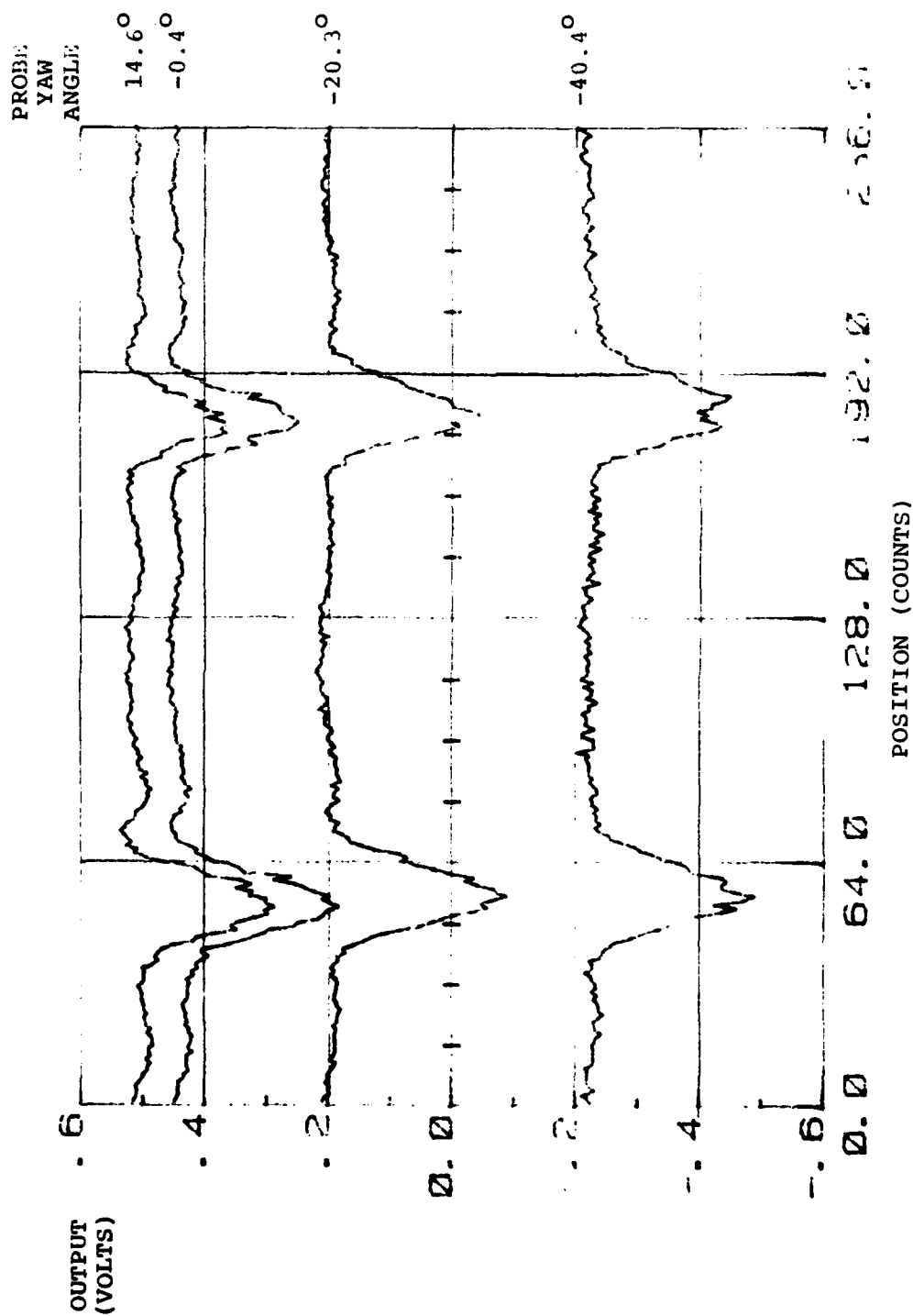
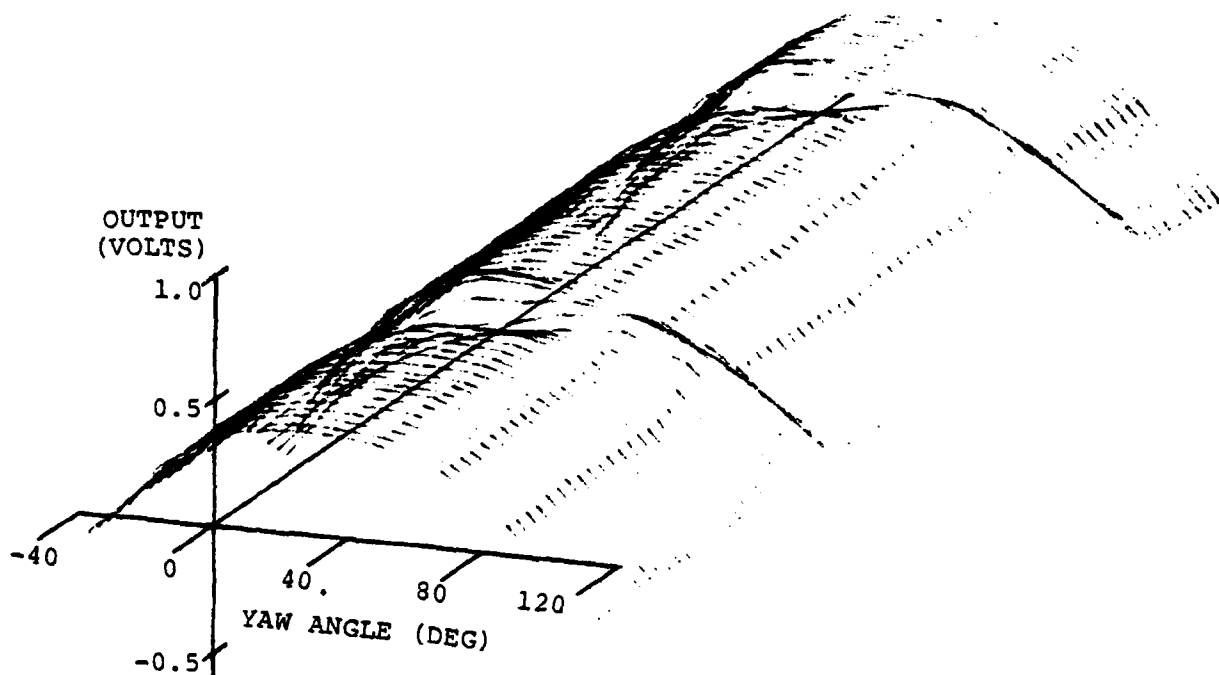
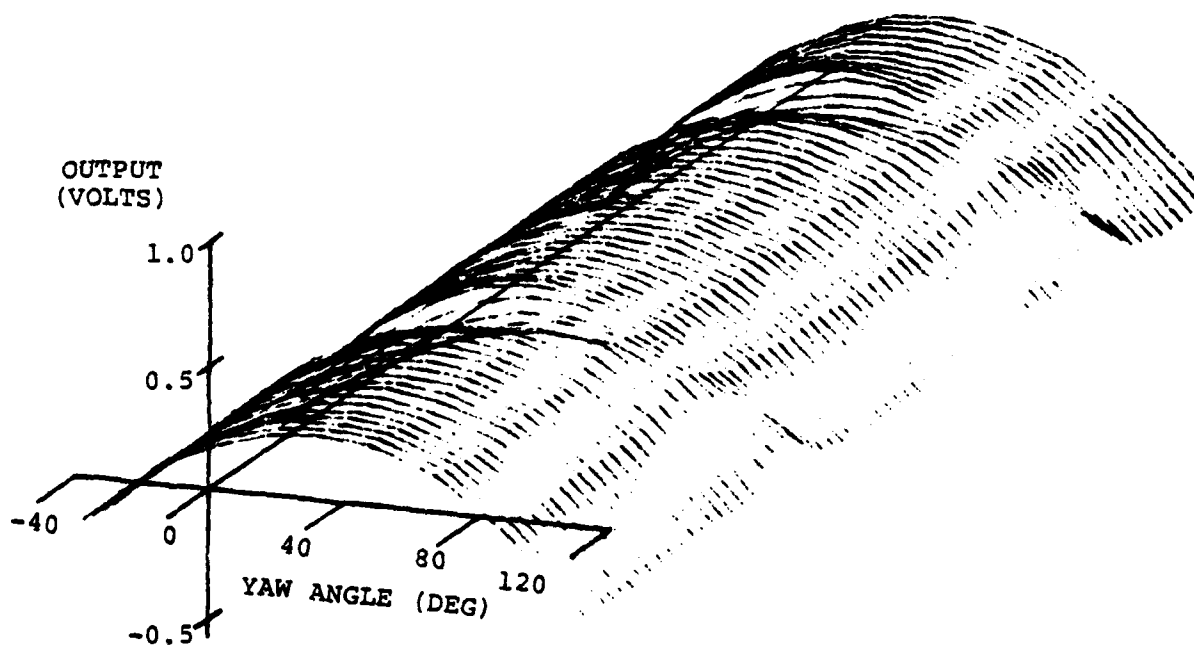


Fig. 5. Examples of Data from the Type A Probe



(a) Type A Probe



(b) Type B Probe

Fig. 6. Total Ensemble Averaged DPDS Data Acquired at One Radial Position for Two Blade Passages

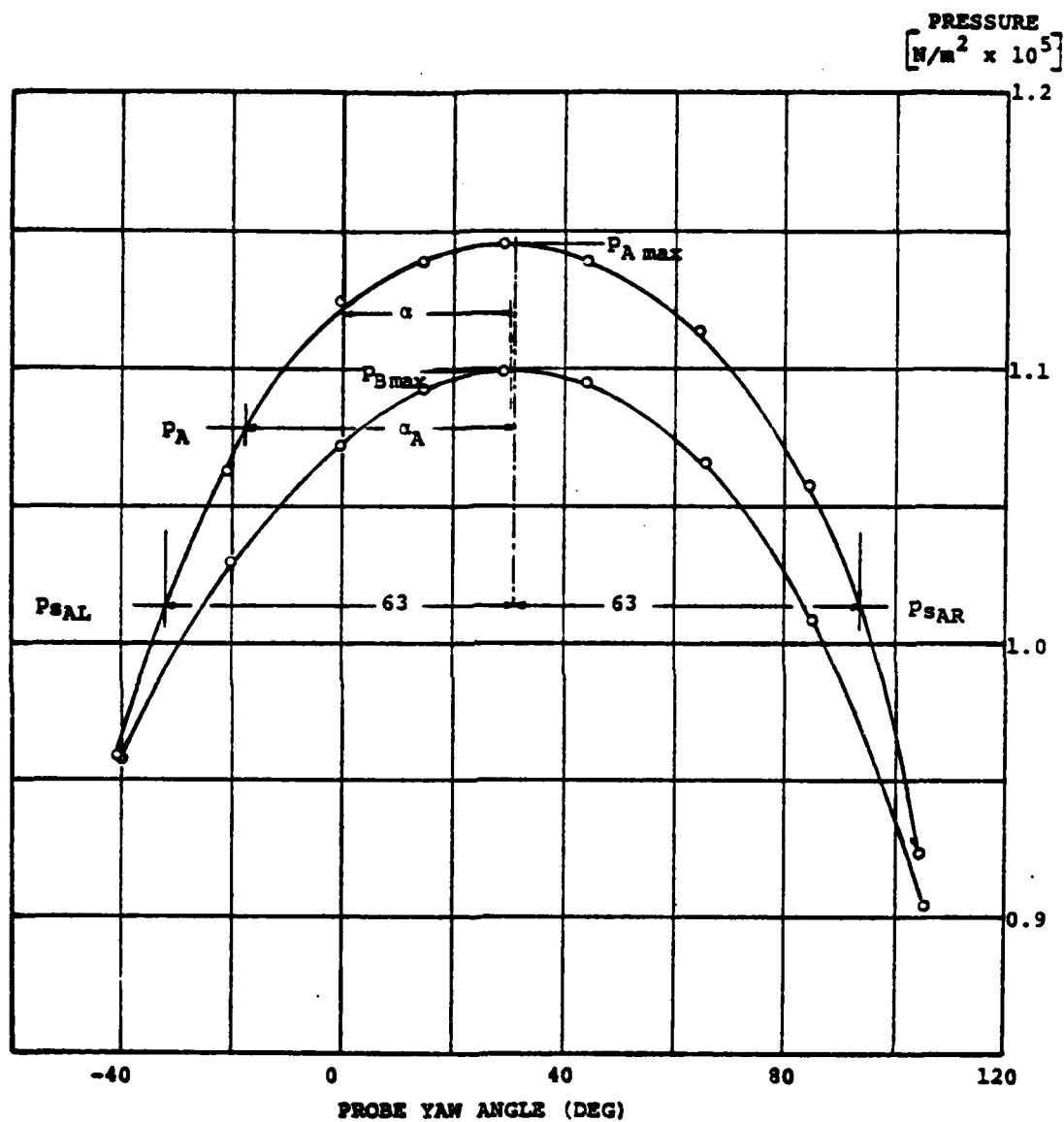


Fig. 7. Example of Data at One Blade-to-Blade Location

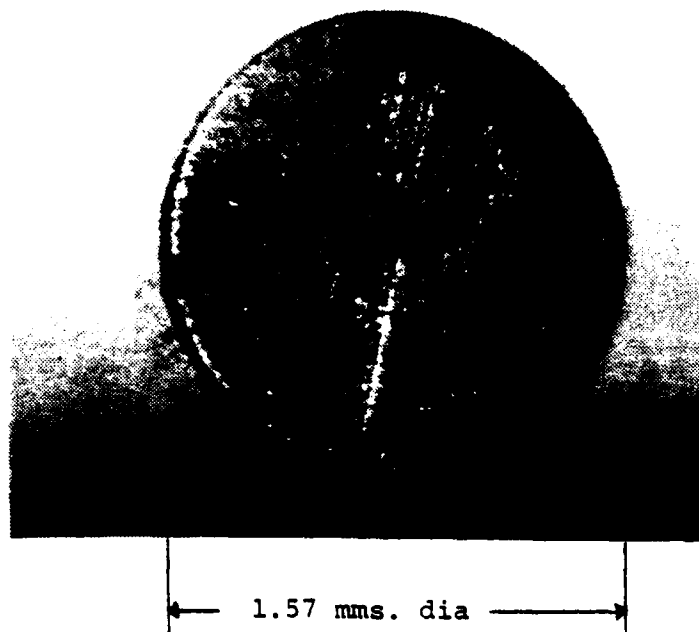


Fig. 8. Second Generation Probe Tip Geometry

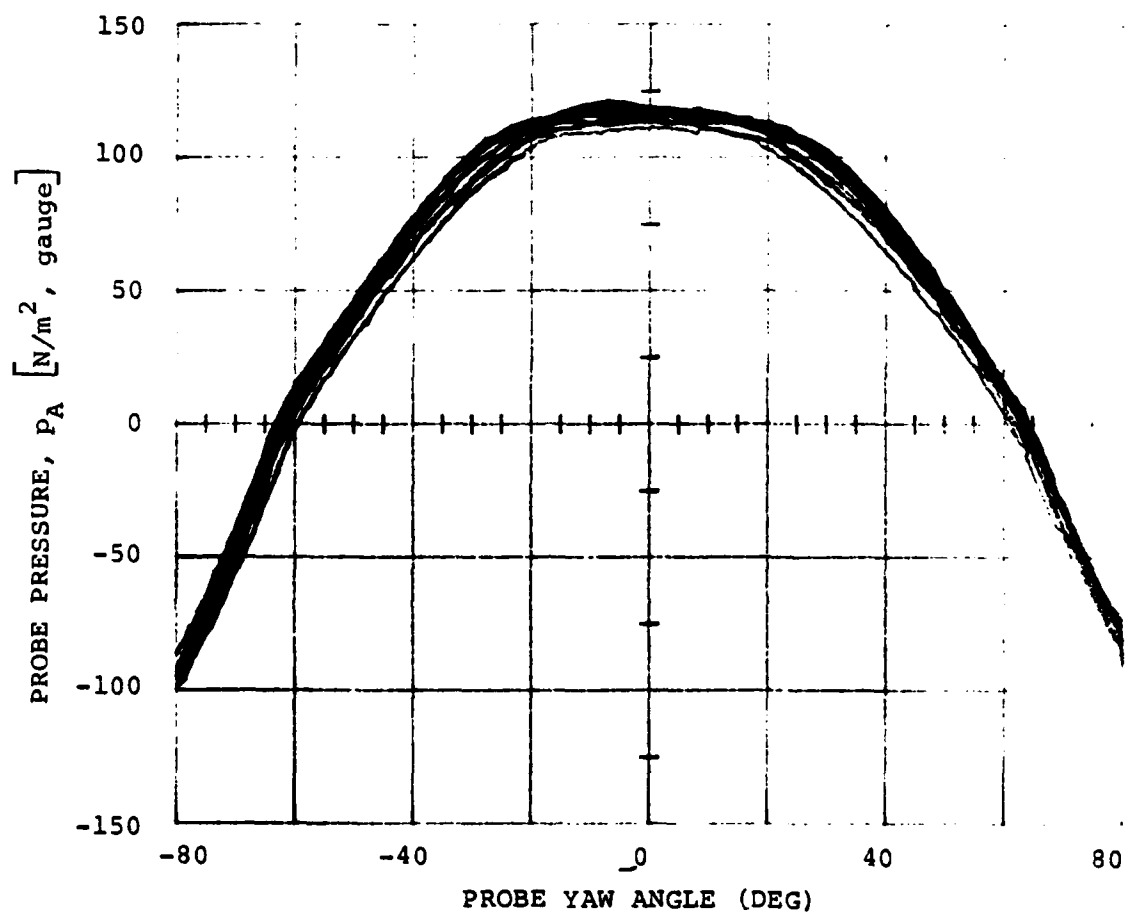


Fig. 9(a). Type A Probe Calibration Data at  $M = 0.4$  and 9 Pitch Angles from  $-15^\circ$  to  $+25^\circ$

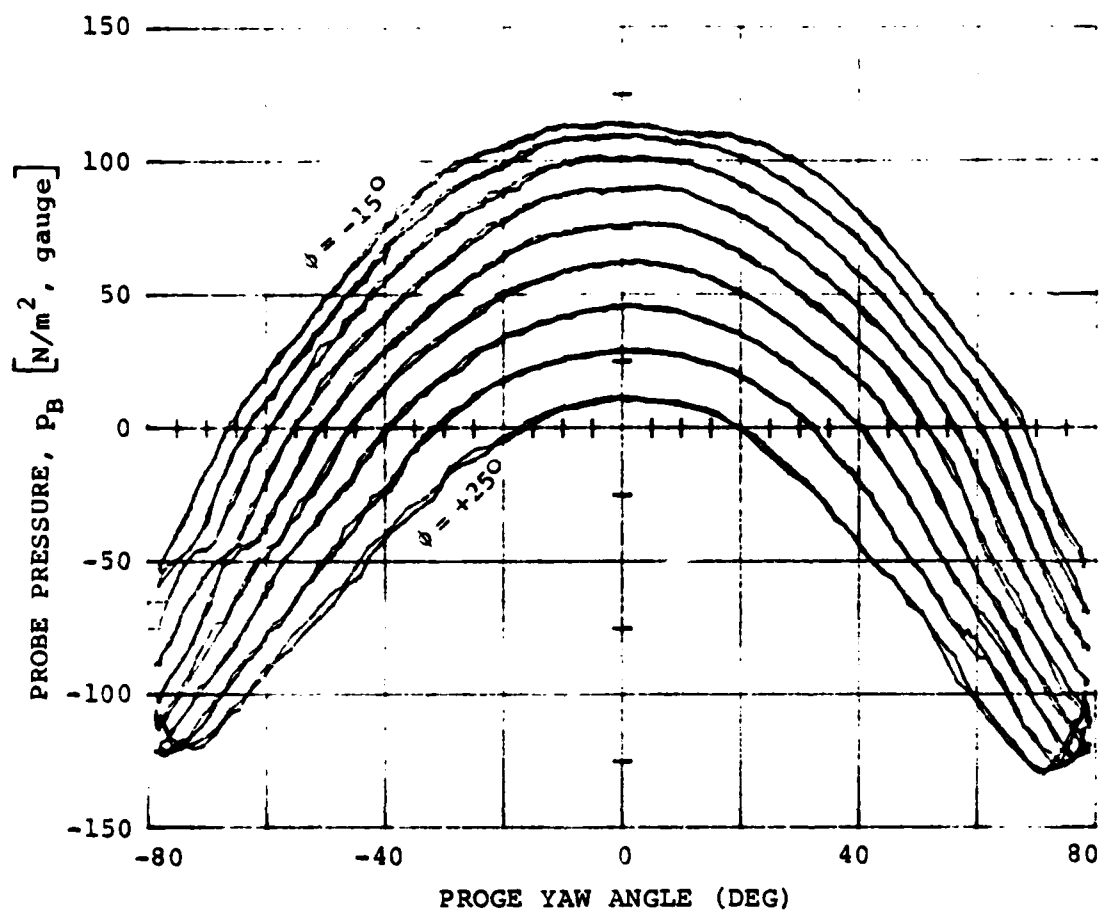


Fig. 9(b). Type B Probe Calibration Data at  $M = 0.4$  and 9 Pitch Angles from  $-15^\circ$  to  $+25^\circ$

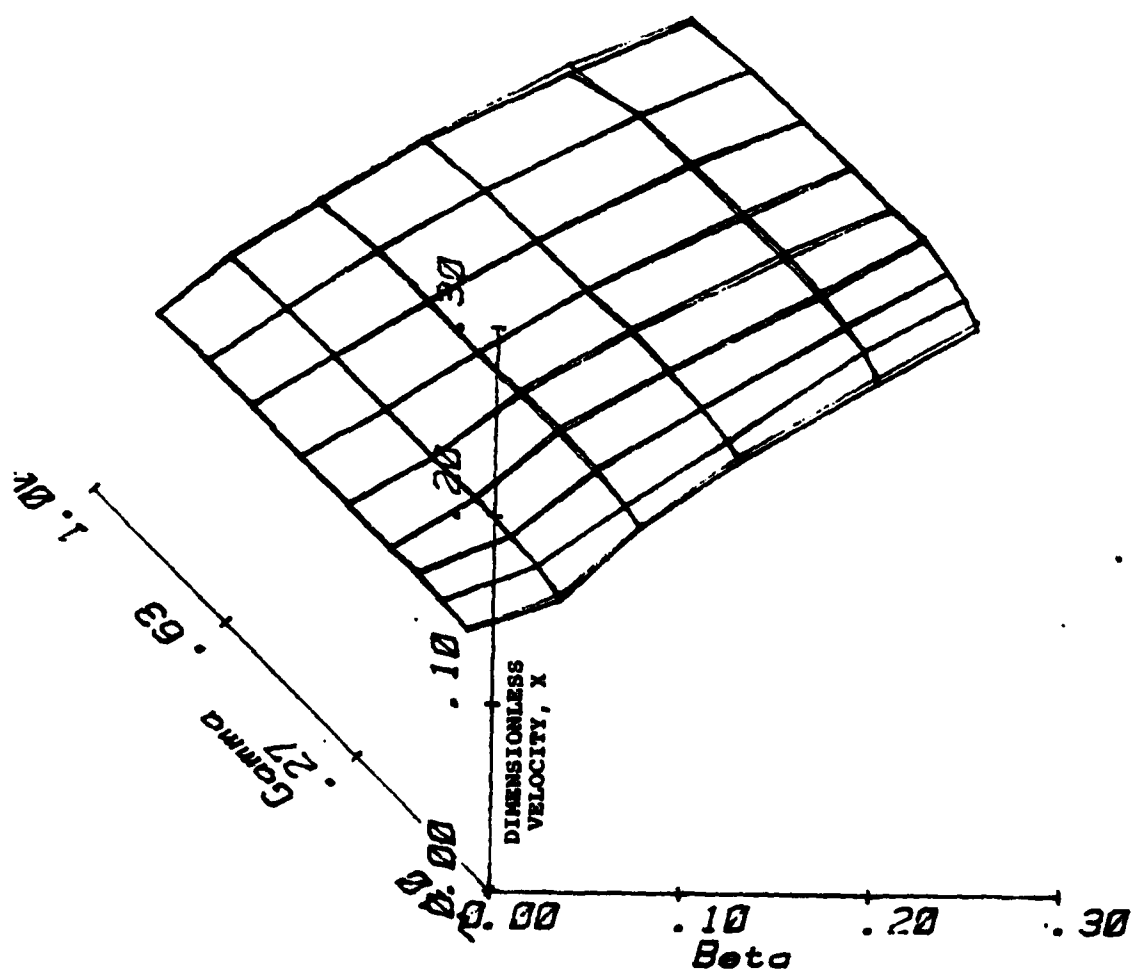


Fig. 10(a). Calibration Surface for Dimensionless Velocity



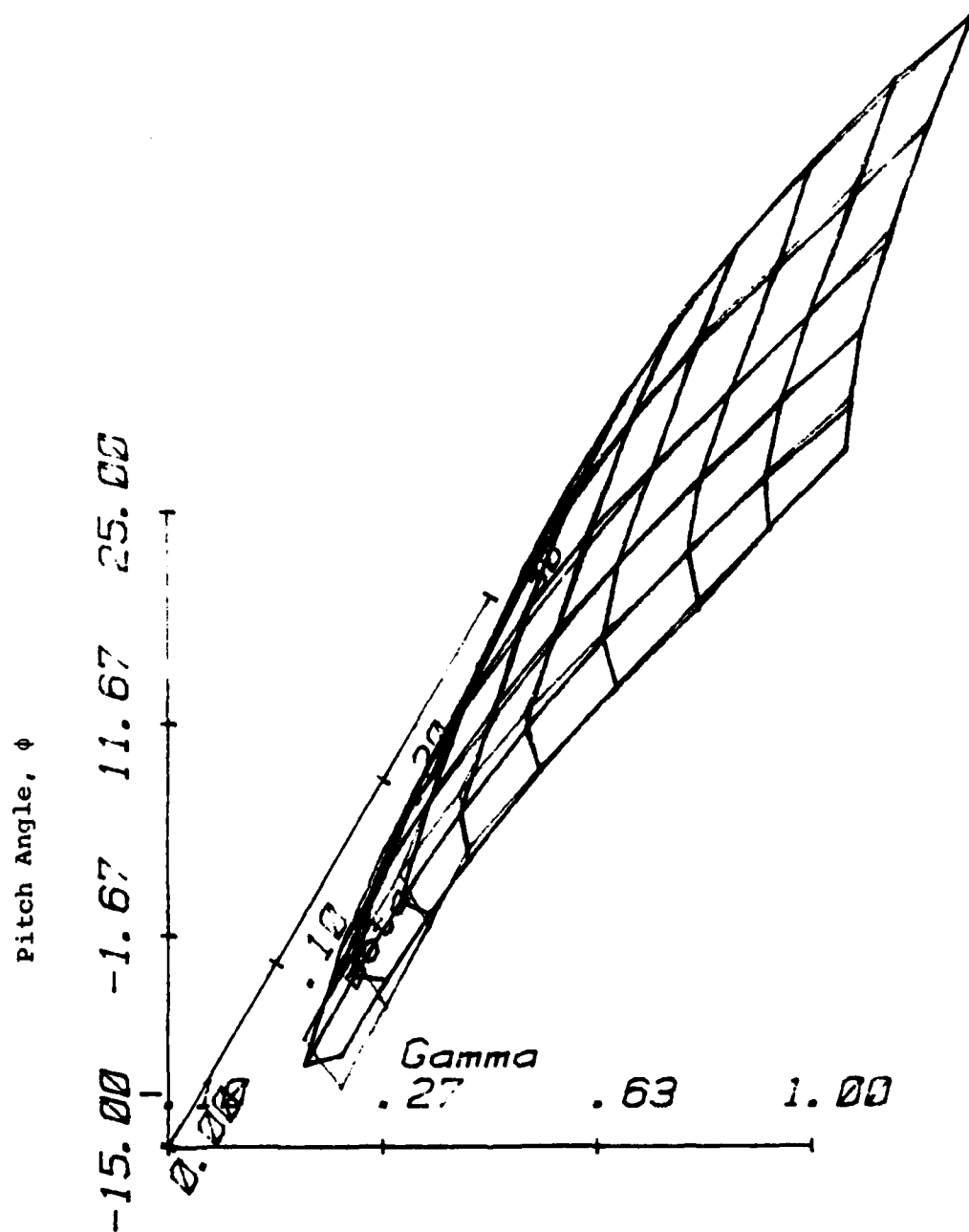
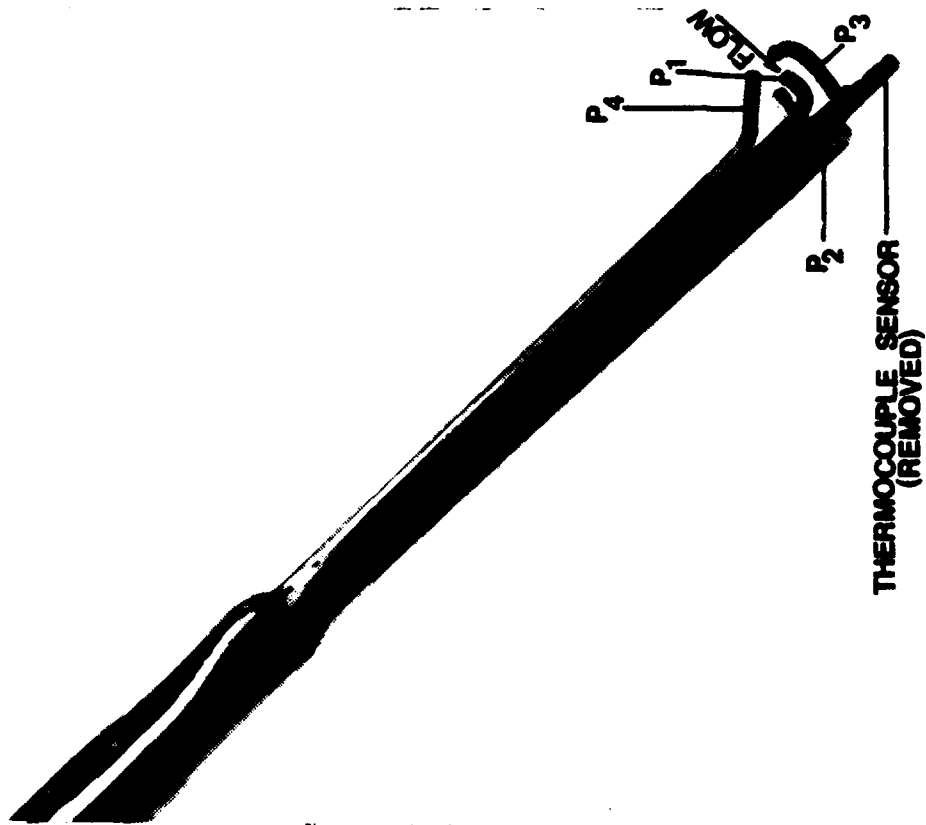


Fig. 10(b). Calibration Surface for Pitch Angle



Scale 20X

Figure 11. Views of the Combination Probe  
(Left - With Thermocouple Sensor Removed. Right - Thermocouple Sensor)

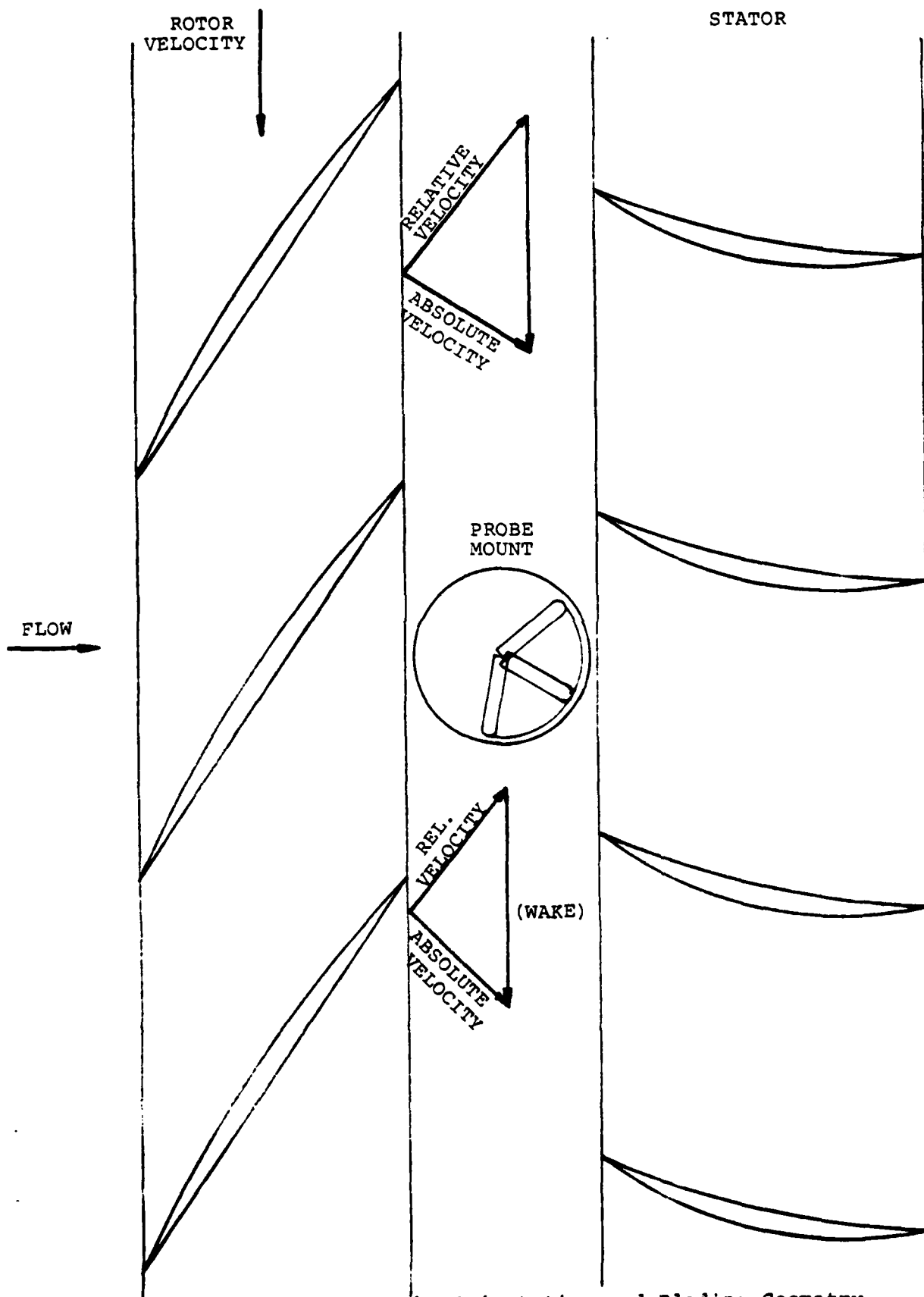


Fig. 12. Probe Orientation and Blading Geometry at the Outer Case Wall

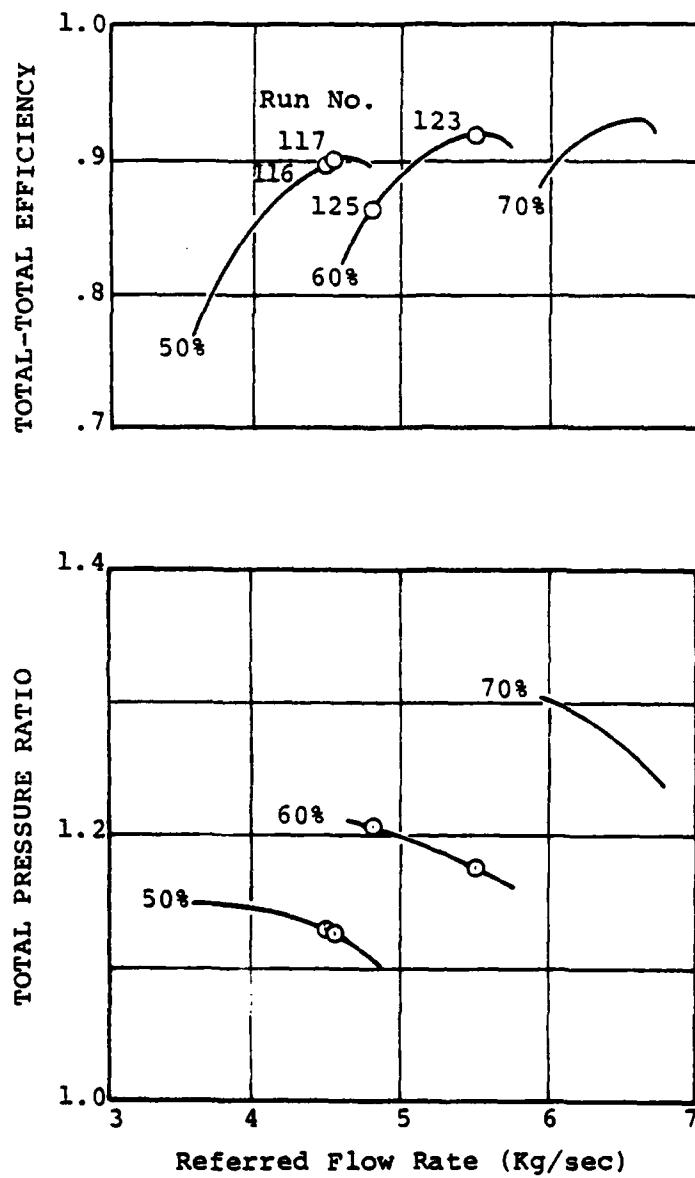


Fig. 13. Compressor Stage Performance at 50, 60 and 70% of Design Speed (30,460 RPM)

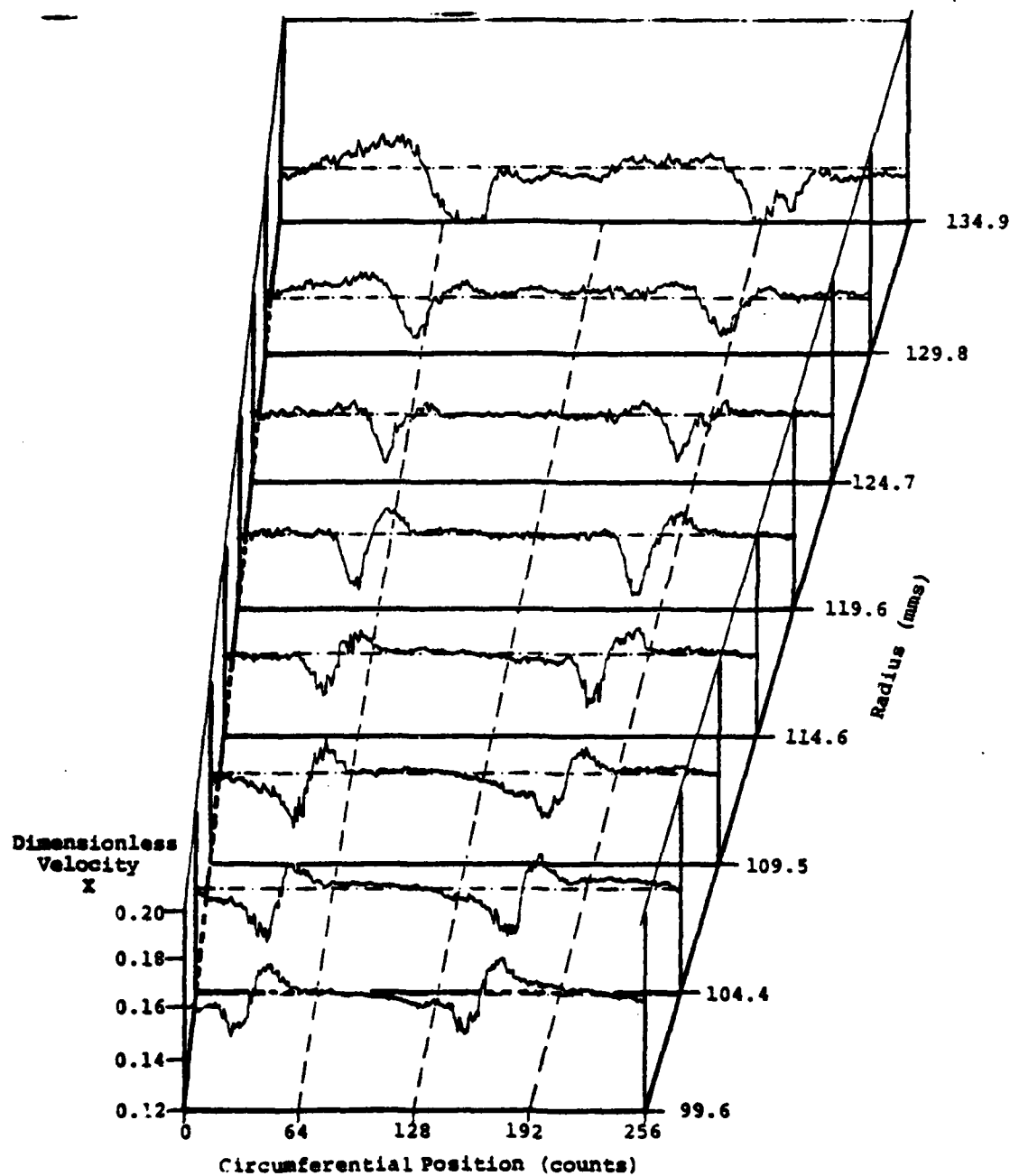


Fig. 14(a). Flow Field from Compressor Rotor Using DPDS Technique at 50% Speed Near Peak Efficiency--Results for Dimensionless Velocity

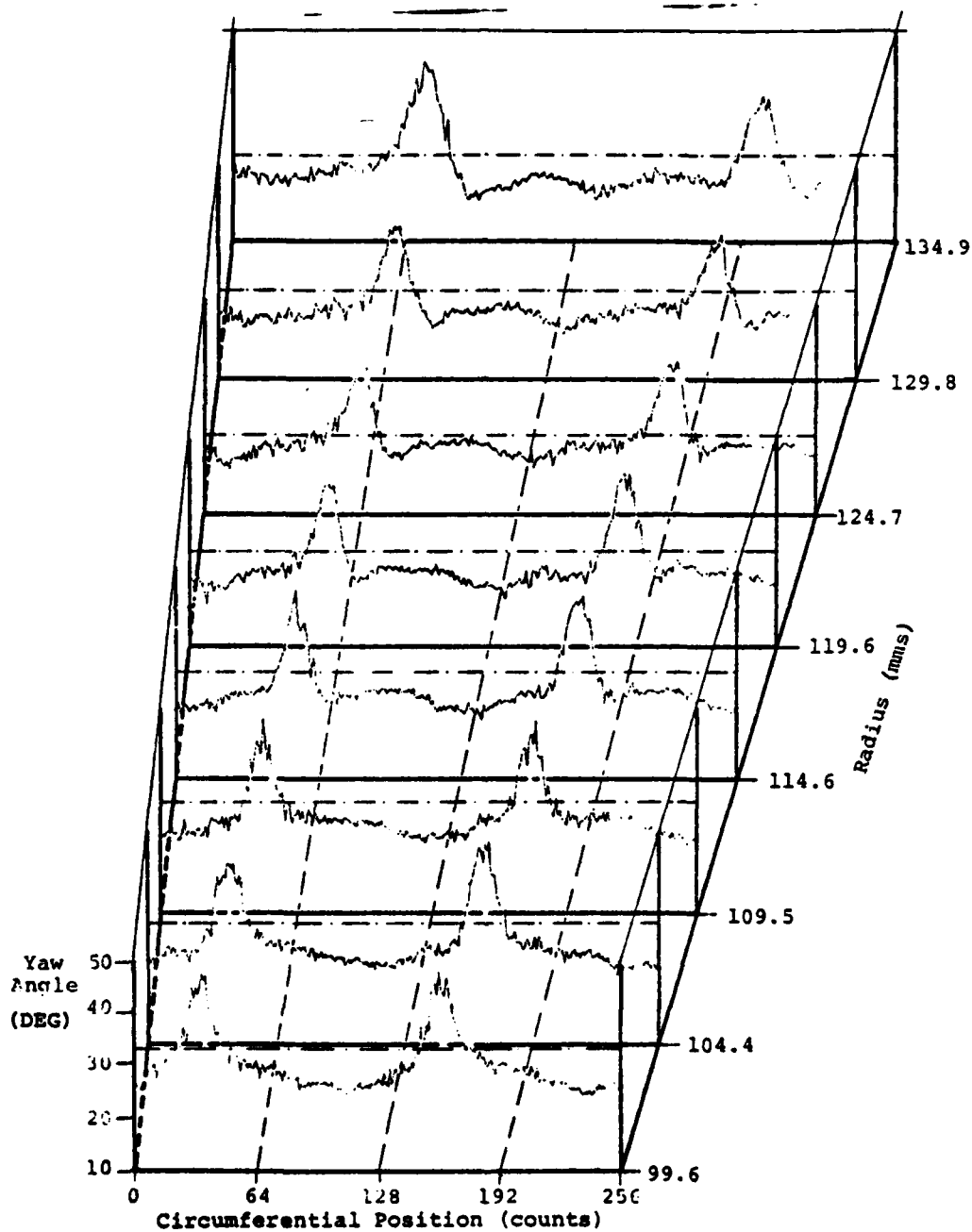


Fig. 14(b). Flow Field from Compressor Rotor Using DPDS Technique at 50% Speed Near Peak Efficiency--Results for Yaw Angle

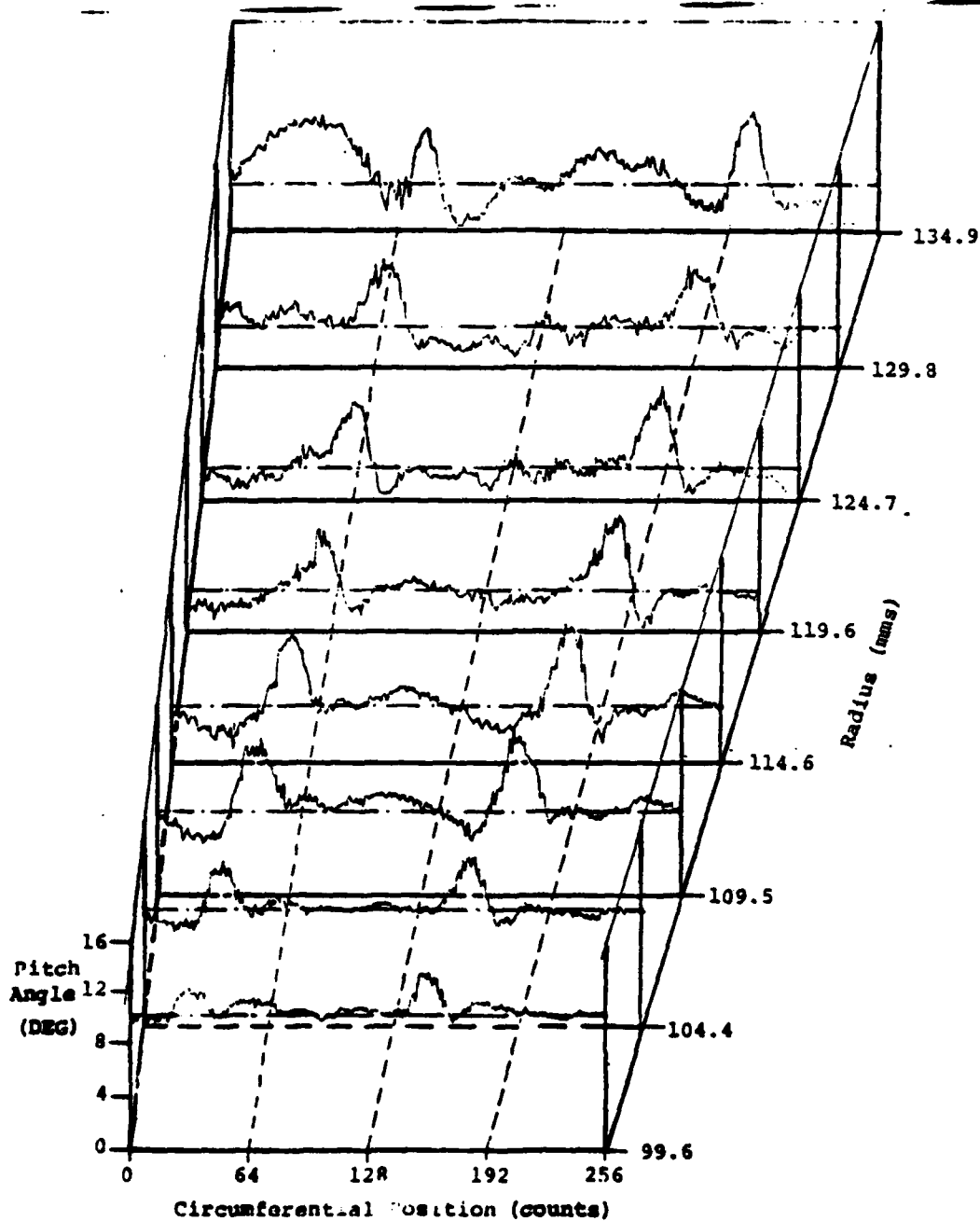


Fig. 14(c). Flow Field from Compressor Rotor Using DPDS Technique at 50% Speed Near Peak Efficiency--Results for Pitch Angle

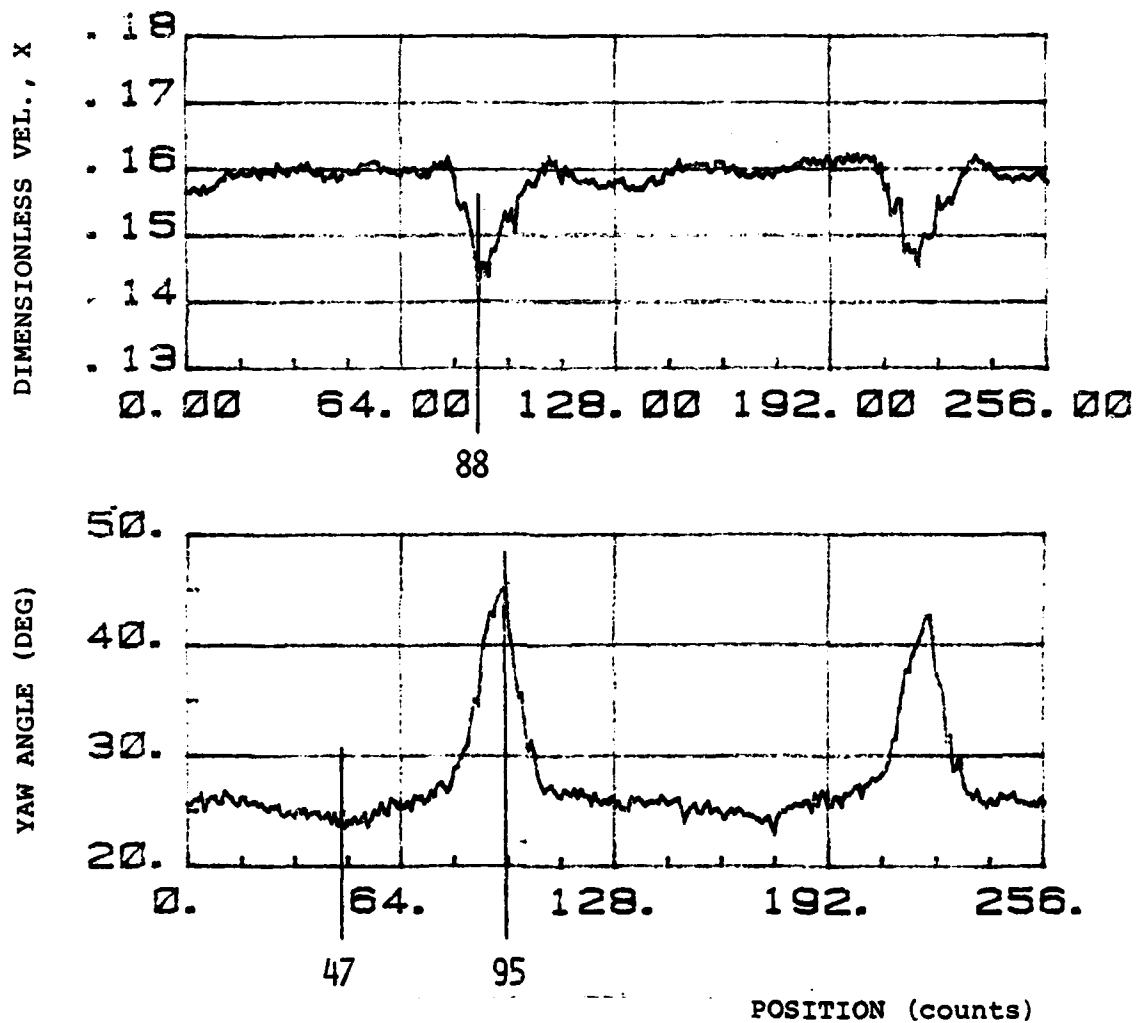


Fig. 15. Measurements at Mid Span at 50% Speed  
(RUN 116, near peak efficiency)



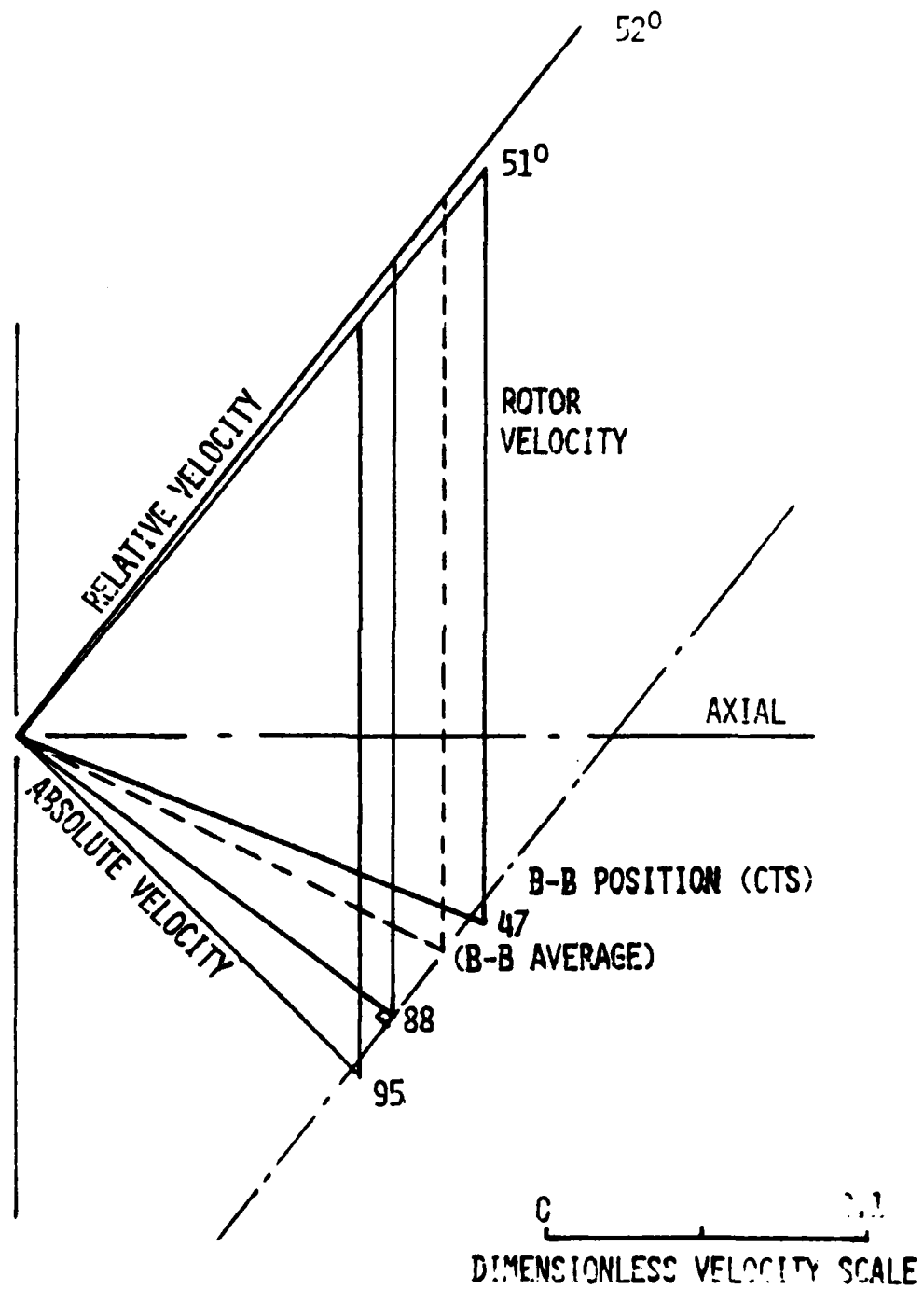


Fig. 16. Velocity Diagrams for Different Blade-Blade Positions

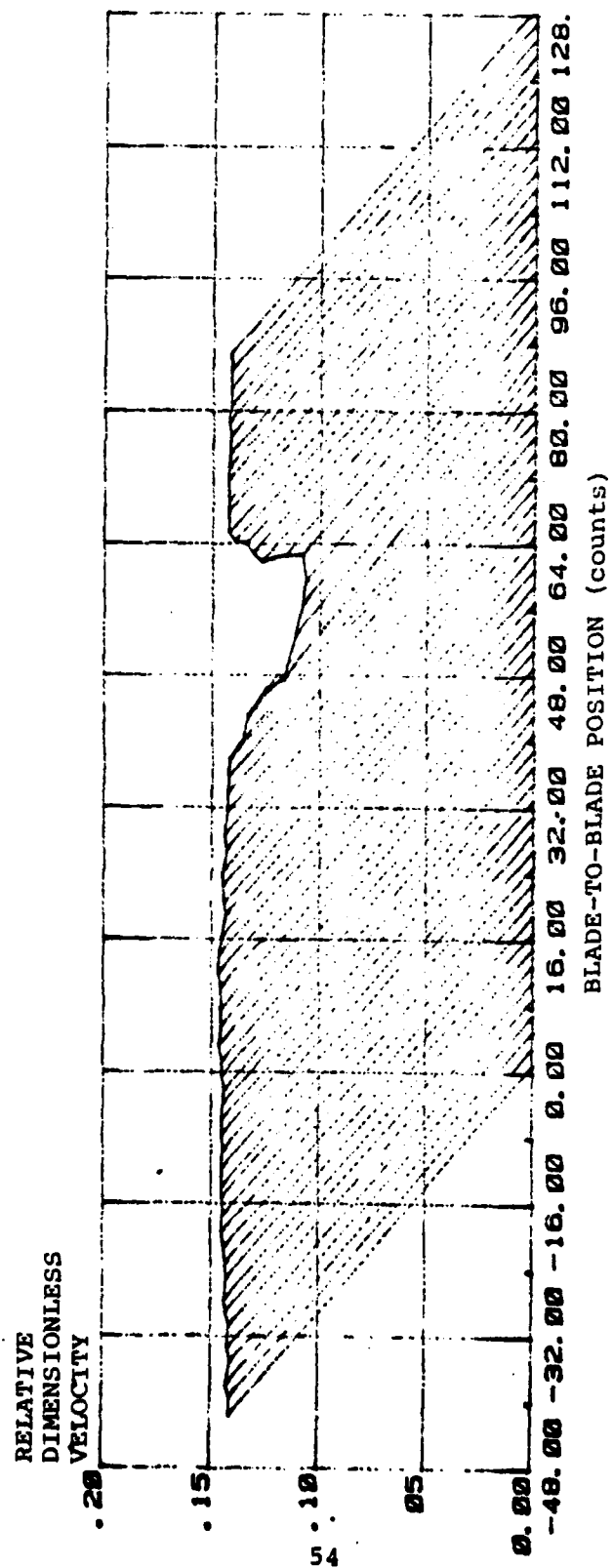


Fig. 17. Relative Flow Velocity Distribution at Mid Span  
Deduced from Absolute Measurements (RUN 116)

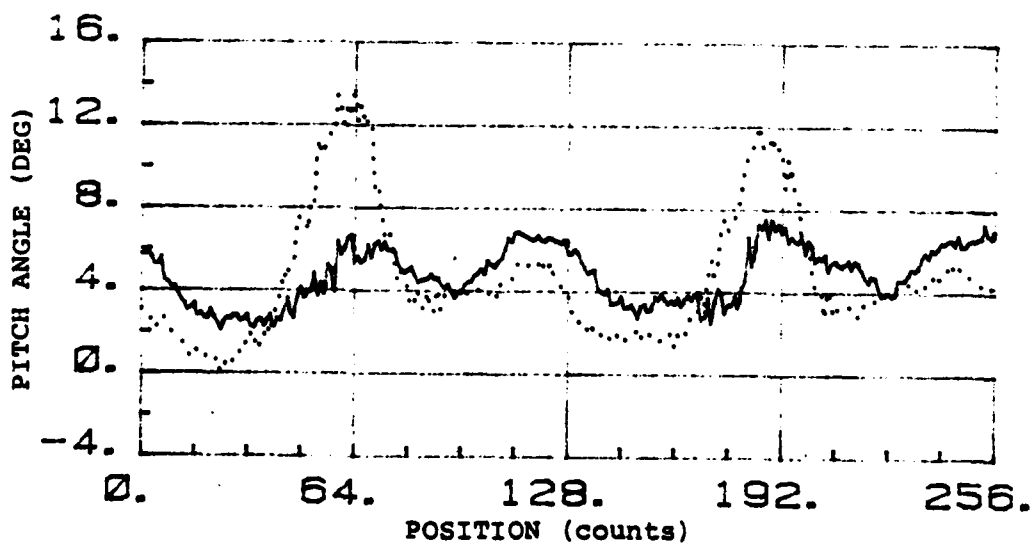
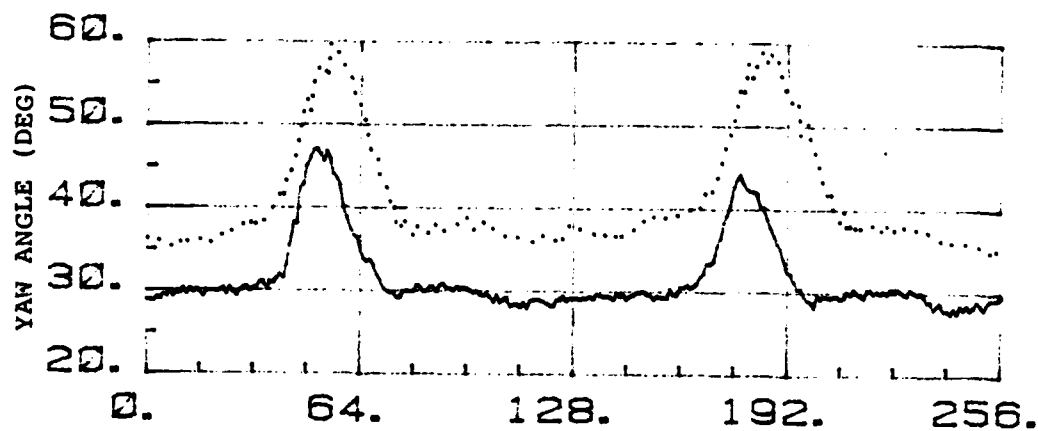
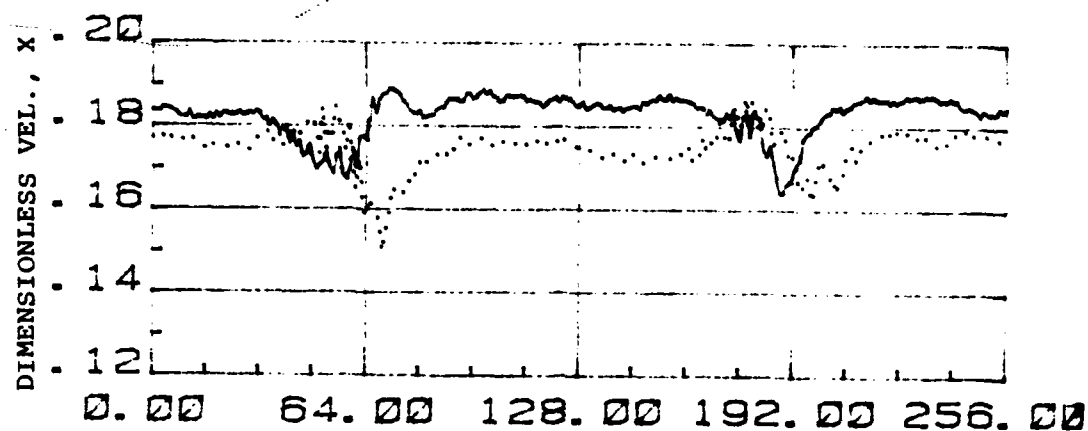


Fig. 18. Second Generation Probe Measurements at Mid Span at 60% Speed (— RUN 123, peak off; ... RUN 125, Throttled)

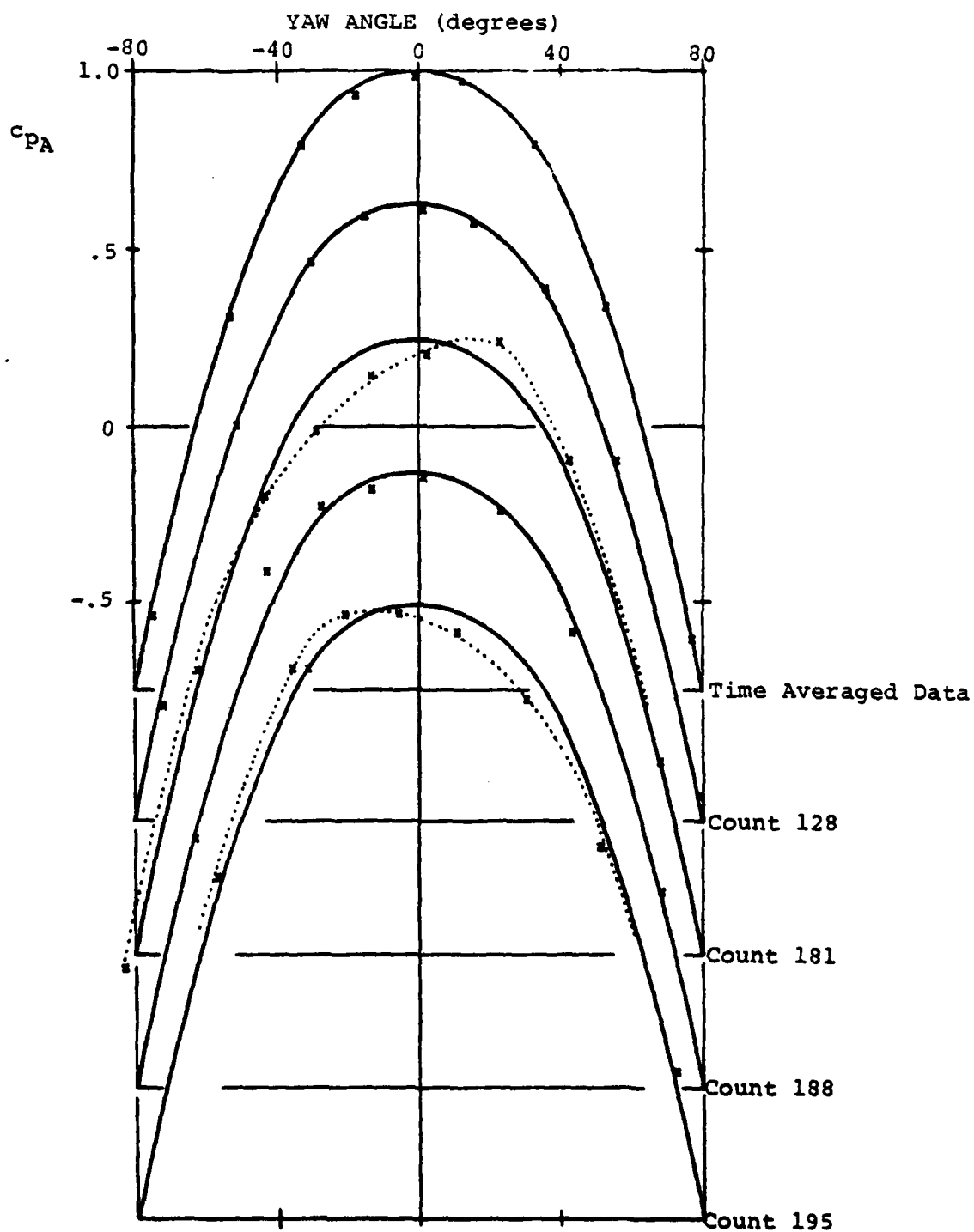


Fig. 19. Pressure Coefficient vs Yaw Angle for Type A Probe at Specific Blade-to-Blade Positions (Run 123. Solid Line is from Calibration at  $m = 0.4, \phi = 0^\circ$ )

#### LIST OF REFERENCES

1. Kerrebrock, J. L., "Flow in Transonic Compressors," AIAA Journal, Vol. 19, No. 1, January 1981.
2. Thompkins, W. T. Jr., "A FORTRAN Program for Calculating Three-Dimensional, Inviscid, Rotational Flows with Shock Waves in Axial Compressor Blade Rows--Users Manual," NASA Contractor Report 3560, June 1982.
3. Shreeve, R. P. et al, Naval Postgraduate School Technical Report (in preparation).
4. Shreeve, R. P., Dodge, F. J., Hawkins, W. R., and Larson, V. J., "Probe Measurements of Velocity and Losses from a Small Axial Transonic Rotor," AIAA Paper No. 78-1198, AIAA 11th Fluid & Plasma Dynamics Conference, Seattle, Washington, July 10-12, 1978.
5. Shreeve, R. P., Simmons, J. M., Winters, K. A., and West, J. C. Jr., "Determination of Transonic Compressor Flow Field by Synchronized Sampling of Stationary Fast Response Transducers," Symposium on Non-Steady Dynamics, ASME 1978 Winter Annual Meeting, San Francisco, California, December 1978.
6. Shreeve, R. P., McGuire, A. G., and Hammer, J. A., "Calibration of a Two-Probe Synchronized Sampling Technique for Measuring Flows Behind Rotors," IEEE International Congress on Instrumentation in Aerospace Simulation Facilities, Monterey, California, September 24-26, 1979. Published in ICIASF '79 Record, IEEE Cat. No. 79CH1500-8AES.
7. Adler, D., and Taylor, P. M., "A Procedure for Obtaining Velocity Vector from Two High Response Impact Pressure Probes," Naval Postgraduate School Technical Report NPS-67-80-007, August 1980.
8. Neuhooff, F., "Further Development of a Dual-Probe Digital Sampling (DPDS) Technique for Measuring Flow Fields in Rotating Machines," Naval Postgraduate School Contractor Report, NPS67-82-01CR, September 1982.
9. Zebner, H., "Procedure and Computer Program for the Approximation of Data (with Application to Multiple Sensor Probes), Naval Postgraduate School Contractor Report, NPS-67-80-01CR, August 1980.

10. Neuhoff, F., "Calibration and Application of a Combination Temperature-Pneumatic Probe for Velocity and Rotor Loss Distribution Measurements in a Compressor," Naval Postgraduate School Contractor Report, NPS67-81-03CR, December 1981.
11. Vavra, M. H., "Design Report of Hybrid Compressor and Associated Test Rig," Naval Postgraduate School Technical Report, NPS-57Va73071A, July 1973.
12. Zebner, H., "Transonic Compressor: Program System TXCO for Data Acquisition and On-Line Reduction," Naval Postgraduate School Contractor Report, NPS67-80-02CR, October 1980.

# DISTRIBUTION LIST

	<u>No. of Copies</u>
1. Library Code 0212 Naval Postgraduate School Monterey, California 93940	4
2. Office of Research Administration Code 012A Naval Postgraduate School Monterey, California 93940	1
3. Chairman Code 67 Department of Aeronautics Naval Postgraduate School Monterey, California 93940	1
4. Director, Turbopropulsion Laboratory Department of Aeronautics Naval Postgraduate School Monterey, California 93940	30
5. Dr. Gerhard Heiche Naval Air Systems Command Code AIR-310 Navy Department Washington, D.C. 20360	1
6. Mr. Karl H. Guttman Naval Air Systems Command Code AIR-330 Navy Department Washington, D.C. 20360	1
7. Dr. A. D. Wood Office of Naval Research 800 North Quincy Street Arlington, Virginia 22217	1
8. Commanding Officer Naval Air Propulsion Test Center Attn: Mr. Vernon Lubosky Trenton, New Jersey 08628	1

9. National Aeronautics & Space Administration 1  
Lewis Research Center (Library)  
2100 Brookpark Road  
Cleveland, Ohio 44135
10. CAG Library 1  
The Boeing Company  
Seattle, Washington 98124
11. Library 1  
General Electric Company  
Aircraft Engine Technology Division  
DTO Mail Drop H43  
Cincinnati, Ohio 45215
12. Library 1  
Pratt and Whitney Aircraft  
Post Office Box 2691  
West Palm Beach, Florida 33402
13. Library 1  
Pratt and Whitney Aircraft  
East Hartford, Connecticut 06108
14. Chief, Fan and Compressor Branch 1  
Mail Stop 5-9  
NASA Lewis Research Center  
2100 Brookpark Road  
Cleveland, Ohio 44135
15. Prof. D. Adler 1  
Technion Israel Institute of Technology  
Department of Mechanical Engineering  
Haifa 32000  
ISRAEL
16. Director, Whittle Laboratory 1  
Department of Engineering  
Cambridge University  
ENGLAND
17. Prof. F. A. E. Breugelmans 1  
Institut von Karman de la Dynamique  
des Fluides  
72 Chaussee de Waterloo  
1640 Rhode-St. Genese  
BELGIUM
18. Library 1  
Air Research Mfg. Corporation  
Division of Garrett Corporation  
402 South 36th Street  
Phoenix, Arizona 85034



19. Prof. Jacques Chauvin 1  
Universite D'Aix-Marseille  
1 Rue Honnorat  
Marseille, FRANCE
  
20. Mr. James V. Davis 1  
Teledyne CAE  
1330 Laskey Road  
Toledo, Ohio 43601
  
21. Dr. Robert P. Dring 1  
United Technologies Research Labs  
400 Main Street  
Hartford, Connecticut 06108
  
22. Mr. Jean Fabri 1  
ONERA  
29, Ave. de la Division Leclerc  
92 Chatillon  
FRANCE
  
23. Prof. Dr. Ing Heinz E. Gallus 1  
Lehrstuhl und Institut fur Strahlantriebe  
und Turbourbeitsmashinen  
Rhein.-Westf. Techn. Hochschule Aachen  
Templergraben 55  
5100 Aachen, WEST GERMANY
  
24. Professor J. P. Gostelow 1  
School of Mechanical Engineering  
The New South Wales Institute of Technology  
AUSTRALIA
  
25. Dr. Ing. Hans-J. Heinemann 1  
DFVLR-AVA  
Bunsenstrasse 10  
3400 Gottingen, WEST GERMANY
  
26. Professor Ch. Hirsch 1  
Vrije Universiteit Brussel  
Pleinlaan 2  
1050 Brussels, BELGIUM
  
27. Chairman 1  
Aeronautics and Astronautics Department  
31-265 Massachusetts Institute of Technology  
Cambridge, Massachusetts 02139
  
28. Dr. B. Lakshminarayana 1  
Professor of Aerospace Engineering  
The Pennsylvania State University  
233 Hammond Building  
University Park, Pennsylvania 16802

29. Mr. R. A. Langworthy 1  
Army Aviation Material Laboratories  
Department of the Army  
Fort Eustis, Virginia 23604
30. Prof. Dr. L. G. Napolitano 1  
Director, Institute of Aerodynamics  
University of Naples  
Viale C. Augusto  
80125 Napoli  
ITALY
31. Prof. Erik Nilsson 1  
Institutionen for Stromningsmaskinteknik  
Chalmers Tekniska Hogskola  
Fack, 402 20 Goteborg 5  
SWEDEN
32. Prof. Gordon C. Oates 1  
Department of Aeronautics and Astronautics  
University of Washington  
Seattle, Washington 98105
33. Prof. Walter F. O'Brian 1  
Mechanical Engineering Department  
Virginia Polytechnic Institute and  
State University  
Blacksburg, Virginia 24061
34. Dr. P. A. Paranjee 1  
Head, Propulsion Division  
National Aeronautics Laboratory  
Post Bag 1799  
Bangalore - 17, INDIA
35. R. E. Peacock, Code 67Pc 1  
Department of Aeronautics  
Naval Postgraduate School  
Monterey, California 93940
36. Dr. W. Schlachter 1  
Brown, Boveri Company Ltd.  
Dept. T-T  
P.O. Box CH-5401 Baden  
SWITZERLAND
37. Prof. T. H. Okiishi 1  
Professor of Mechanical Engineering  
208 Mechanical Engineering Building  
Iowa State University  
Ames, Iowa 50011

38. Dr. Fernando Sisto 1  
Professor and Head of Mechanical  
Engineering Department  
Stevens Institute of Technology  
Castle Point, Hoboken, New Jersey 07030
39. Dr. Leroy H. Smith, Jr. 1  
Manager, Compressor and Fan  
Technology Operation  
General Electric Company  
Aircraft Engine Technology Division  
DTO Mail Drop H43  
Cincinnati, Ohio 45215
40. Dr. W. Tabakoff 1  
Professor, Department of Aerospace  
Engineering  
University of Cincinnati  
Cincinnati, Ohio 45221
41. Mr. P. Tramm 1  
Manager, Research Labs  
Detroit Diesel Allison Division  
General Motors  
P.O. Box 894  
Indianapolis, Indiana 46206
42. Prof. Dr. W. Traupel 1  
Institut fur Thermische Turbomaschinen  
Eidg. Technische Hochschule  
Sonneggstrasse 3  
8006 Zurich, SWITZERLAND
43. Dr. Arthur J. Wennerstrom 1  
ARL/LF  
Wright-Patterson AFB  
Dayton, Ohio 45433
44. Dr. H. Weyer 1  
DFVLR  
Linder Hohe  
505 Porz-Wahn  
WEST GERMANY
45. Mr. P. F. Yaggy 1  
Director  
U.S. Army Aeronautical Research Laboratory  
AMES Research Center  
Moffett Field, California 94035

46. Prof. C. H. Wu 1  
P.O. Box 2706  
Beijing 100080  
CHINA
47. Director 1  
Gas Turbine Establishment  
P.O. Box 305  
Jiangyou County  
Sichuan Province  
CHINA
48. Professor Leonhard Fottner 1  
Department of Aeronautics and Astronautics  
German Armed Forces University  
Hochschule des Bundeswehr  
Werner Heisenbergweg 39  
8014 Neubiberg near Munich  
WEST GERMANY
49. Dr. G. J. Walker 1  
Civil and Mechanical Engineering  
Department  
The University of Tasmania  
Box 252C  
GPO Hobart  
Tasmania, AUSTRALIA 7001

LATE  
LME